Chen *et al. Stem Cell Research & Therapy* (2025) 16:116
https://doi.org/10.1186/s13287-025-04228-2

Stem Cell Research & Therapy

RESEARCH Open Access

Mesenchymal stem cell-derived small extracellular vesicles reduced hepatic lipid accumulation in MASLD by suppressing mitochondrial fission

Yifei Chen[1,2†], Fuji Yang[1,2†], Yanjin Wang[1,2], Yujie Shi[1,2], Likang Liu[1,2], Wei Luo[3,4], Jing Zhou[3,4] and Yongmin Yan[1,3,4*]

Abstract

Background Metabolic dysfunction-associated steatotic liver disease (MASLD) is a chronic liver disease characterized by lipid accumulation in liver cells. Human umbilical cord mesenchymal stem cell-derived small extracellular vesicles (MSC-sEV) have great potential in repairing and regenerating liver diseases. However, it is still unclear whether MSC-sEV can inhibit hepatocyte lipid accumulation by regulating mitochondrial fission.

Methods We investigated the effects of MSC-sEV on mitochondrial fission and its potential mechanism in lipotoxic hepatocytes and high-fat diet (HFD)-induced MASLD mice.

Results We found that MSC-sEV can effectively inhibit the expression of the Dynamin-related protein 1 (DRP1), thereby reducing mitochondrial fission, mitochondrial damage, and lipid deposition in lipotoxic hepatocytes and livers of HFD-induced MASLD in mice. Further mechanistic studies revealed that RING finger protein 31 (RNF31) played a crucial role in mediating the inhibitory effect of MSC-sEV on DRP1 and mitochondrial fission. RNF31 can suppress DRP1 expression and mitochondrial fission, thereby improving mitochondrial dysfunction and reducing hepatocyte lipid deposition. These findings suggest that MSC-sEV may downregulate hepatocyte DRP1-mediated mitochondrial fission by transporting RNF31, ultimately inhibiting hepatocyte lipid accumulation.

Conclusions The insights from this study provide a new perspective on the mechanism of MSC-sEV in reducing lipid accumulation and offer a potential therapeutic target by targeting DRP1 to inhibit hepatocyte steatosis and the progression of MASLD.

†Yifei Chen and Fuji Yang contributed equally to this work.

*Correspondence:
Yongmin Yan
yym@wjrmyy.cn

Full list of author information is available at the end of the article

Graphical abstract

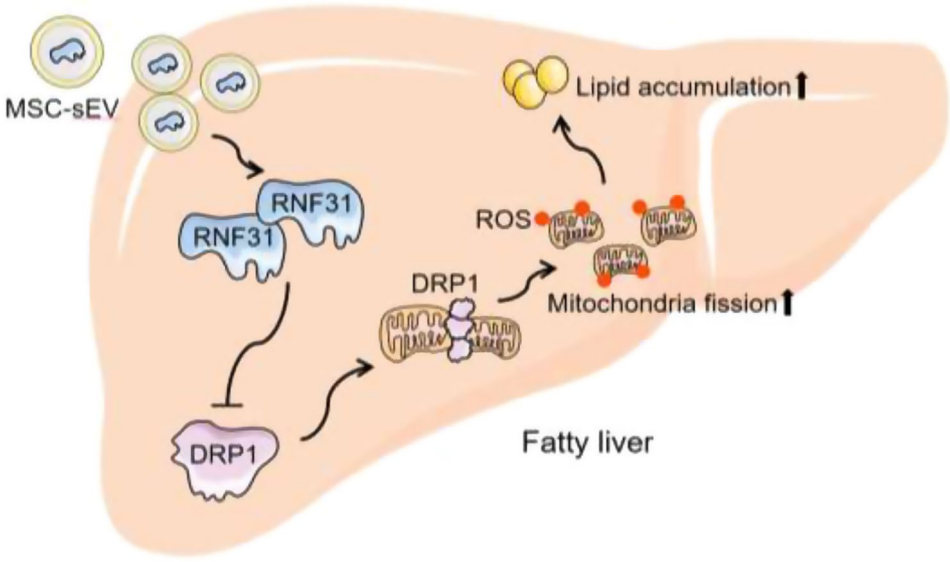

Keywords MASLD, MSC, Small extracellular vesicles, DRP1, Mitochondrial fission

Introduction

Metabolic dysfunction-associated steatotic liver disease (MASLD) is a prevalent chronic disease that significantly impacts the health of individuals worldwide [1]. MASLD not only poses a substantial risk for metabolic dysfunction-associated steatohepatitis (MASH), cirrhosis, and liver cancer but also has strong associations with the increased incidence of type 2 diabetes, cardiovascular disease, osteoporosis, chronic kidney disease, and other related conditions [2–6]. The underlying causes of MASLD remain unclear, although the Food and Drug Administration (FDA) has recently approved resmetirom for treating MASLD [7]. Consequently, it is imperative to explore effective intervention methods for the management of MASLD urgently.

In recent years, there has been a growing utilization of mesenchymal stem cells (MSCs) in the treatment of various clinical liver diseases [8]. Adipose tissue-derived stem cell (ADSC) transplantation has been reported to promote the reversal of non-alcoholic fatty liver disease (NAFLD) by improving liver function and mitigating lipid metabolism and oxidative stress [9, 10]. Additionally, ADSC therapy has demonstrated positive outcomes in the treatment of cirrhosis [11]. Multi-center clinical studies have demonstrated the potential of MSCs in enhancing the condition of patients with cirrhosis by reducing liver inflammation and facilitating the repair of damaged liver tissue [12]. However, the clinical application of MSCs is limited due to safety concerns [13]. Further research has revealed that MSCs primarily function through the paracrine pathway [14], with small extracellular vesicles (MSC-sEV) being a vital component of this pathway. MSC-sEV possesses the functions of MSCs and offers unique advantages such as no immunogenicity and no risk of tumor formation [15]. As a result, MSC-sEV shows excellent potential in treating liver diseases like acute liver injury, MASLD, and liver fibrosis [16].

Previous studies have demonstrated that MSC-sEV, rich in bioactive molecules, possesses significant reparative potential in various diseases, including acute and chronic liver injury, ischemic renal injury, renal fibrosis, and type 2 diabetes [16–19]. In the context of liver injury repair, MSC-sEV has been found to exhibit resistance to oxidation and inhibit hepatocyte apoptosis, thereby rescuing liver failure [20]. Additionally, they contribute to reducing liver fibrosis by promoting hepatic stellate cell ferroptosis and alleviating liver steatosis by enhancing fatty acid oxidation while reducing fatty acid synthesis in hepatocytes [21, 22]. Furthermore, studies have shown that MSC-sEV can prevent MASH induced by a methionine-choline-deficient diet [23]. However, the specific role and mechanism of MSC-sEV in repairing MASLD have yet to be fully elucidated.

Mitochondrial dysfunction plays a crucial role in the progression of MASLD [24]. This dysfunction leads to oxidative stress and energy production disorders in hepatocytes, resulting in the loss of mitochondrial membrane potential and abnormal accumulation of mitochondrial reactive oxygen species (mROS), ultimately contributing to the advancement of MASLD [25]. One key factor

in regulating mitochondrial morphology and movement is dynamin-related protein 1 (DRP1). DRP1 recruits and increases mitochondrial fragmentation on mitochondria, thereby pivotal in maintaining mitochondrial homeostasis [26]. Inhibiting mitochondrial fission has been shown to improve fibrosis in mice and reduces inflammation and oxidative stress [27]. However, the specific role of MSC-sEV in regulating mitochondrial fission and mitochondrial homeostasis in hepatocytes requires further exploration.

RING finger protein 31 (RNF31), sometimes referred to as HOIL-1 interacting protein (HOIP), is classified as an E3 ubiquitin ligase that falls under the category of RING-between-RING (RBR) proteins. Our previous research shows that RNF31 plays a key role in the progression of MASLD by mediating the mitophagy [28]. However, mitochondria require an extensive proteome to maintain a variety of metabolic reactions [29], since RNF31 could influence mitophagy process, so it may also regulate the mitochondrial fission by DRP1 in MASLD.

This study aimed to investigate the role and mechanism of MSC-sEV in inhibiting hepatocyte lipid accumulation and repairing MASLD by regulating mitochondrial fission. In both in vivo and in vitro models, we observed the inhibitory effect of MSC-sEV on the expression of the mitochondrial fission regulatory factor DRP1 and its impact on mitochondrial fission, mROS production, mitochondrial respiration, and lipid deposition in lipotoxic hepatocytes. Furthermore, we delved into the mechanism through which MSC-sEV down-regulates DRP1 expression. The results revealed that RNF31 plays a pivotal role as the active factor in MSC-sEV's inhibition of mitochondrial fission. By reducing the expression of DRP1, RNF31 can effectively inhibit mitochondrial fission and hepatocyte lipid deposition. These findings offer novel insights into the role and mechanism of MSC-sEV in repairing MASLD.

Materials and methods

Cell culture

Human liver hepatocellular carcinoma cell line HepG2 (#CL0137) and human hepatic cell line LO2 (#CL0192) were purchased from Fenghui Biology Co., Ltd (Changsha, China) and cultured in DMEM High Glucose medium (Gibco, USA) and RPMI 1640 (Gibco, USA, C11875500), respectively, containing 10% fetal bovine serum (FBS; ExCell, USA, FND50). HepG2 and LO2 cells were treated with Oleic acid (C18:1; Sigma, USA, O7501) and Palmitic acid (C16:0; Sigma, USA, P0500) at a ratio of 2:1 (1.0 mM OPA) for 24 h to induce lipotoxic injury. The human mesenchymal stem cells (MSCs) were cultured in serum-free α-MEM medium (MEM; Gibco, USA, 12571063) supplemented with 100 U of penicillin/streptomycin (Invitrogen, USA, 15140148). The LO2 cell lines utilized in this study were identified using genotyping of STR loc by Shanghai Yihe Biotechnology Co., Ltd.

Isolation and characterization of MSC-sEV

Human MSCs used in this study were prepared following the methods described in our previous study [30]. MSCs were isolated from fresh umbilical cords with the consent of mothers at the Wujin Hospital Affiliated with Jiangsu University. After the permission of mothers, human umbilical cords were placed in phosphate buffer solution (PBS) containing penicillin-streptomycin for 30 min, followed by the removal of arteries and veins. Subsequently, the umbilical cords were cut into 2-cm pieces, pasted on the bottom of culture dishes, placed upside-down in the culture incubator for 60 min, and maintained in serum-free DMEM (Life Technologies, USA) at 37 °C with 5% CO2. The culture medium was changed every 3 days. Primary cells were trypsinized and passaged for further expansion.

We performed ultracentrifugation to obtain small extracellular vesicles from the conditioned culture supernatant of MSCs (MSC-sEV). Initially, the conditioned culture supernatant was centrifuged at 10,000 g for 30 min to remove cells and cell debris. Subsequently, the concentrated supernatant was ultracentrifuged at 100,000 g for 70 min using an Optima L-90 K ultracentrifuge (Beckman Coulter, Brea, CA). The MSC-sEV-enriched fraction was collected from the bottom of the tube and washed three times with phosphate-buffered saline (PBS) through centrifugation at 1,500 g for 30 min with a 100-KDa MWCO filter. Finally, MSC-sEV was filtered through a 0.22-mm filter and stored at -80 °C. The protein concentration of MSC-sEV was determined using a BCA protein assay kit (CWBIO, Beijing, China), and the expression of exosomal markers TSG101, CD63, CD9, and endoplasmic reticulum protein Calnexin were analyzed by western blot. The morphologies and size distribution of MSC-sEV were examined using transmission electron microscopy (TEM, FEI Tecnai 12, Philips, The Netherlands) and nanoparticle tracking analyses (NTA, ZetaView, Germany).

Uptake of MSC-sEV by HepG2 and LO2 cells

The Dir-labeled MSC-sEV (1.2×10^9 particle/ml) were co-incubated with HepG2 and LO2 cells treated with Oleic acid and Palmitic acid for 24 h. After that, the cells were washed three times with PBS and fixed with 4% paraformaldehyde for 30 min. The nuclei were stained with a 0.1% DAPI solution (ZSGB-BIO, Beijing, China, ZLI-9557). The cellular uptake ability was examined using a Confocal Imaging System microscope (Leica Microsystems, Germany).

Western blot

The cultured cells and livers were lysed in RIPA lysis buffer (Pierce, Rockford, USA) at 4 °C for 30 min. The lysates were loaded on phenylmethylsulfonyl fluoride (PMSF, 10 mM). According to the manufacturer's instructions, the protein concentration was quantified using the BCA Protein Assay Kit (CWBIO, Beijing, China). Subsequently, the samples were analyzed by 10–12% sodium dodecyl sulfate-polyacrylamide gel electrophoresis (SDS-PAGE) and transferred onto a PVDF membrane (IPVH00010, Millipore). The membranes were blocked in TBS/T containing 5% defatted milk for 1 h. After that, the membranes were incubated with primary antibody at 4 °C for at least 12 h in TBS/T containing 5% BSA. The antibodies used were as follows: CD9 (1:1000, Bioworld, USA, BS3022), CD63 (1:1000, Abcam, UK, ab271286), TSG101 (1:1000, Bioworld, USA, BS91381), Calnexin (1:1000, Bioworld, USA, BS1438), DRP1 (1:4000, ABclonal, Wuhan, China, A2586), RNF31 (1:1000, Bioworld, USA, BS71127), FIS1 (1:1000, ABclonal, Wuhan, China, A5821), TRAF7 (1:1000, ABclonal, Wuhan, China, A3095), UBC (1:1000, ABclonal, Wuhan, China, A3207) and β-actin (1:2000, ABclonal, Wuhan, China, AC006). Subsequently, the membranes were incubated with HRP-conjugated secondary antibodies (1:2000, Invitrogen, USA, 31460) at room temperature for 1 h. The protein bands were visualized using electrochemiluminescence (Vazyme, Nanjing, China, E412-01).

Mitochondrial staining

The structure of mitochondria in HepG2 and LO2 cells was visualized using a MitoTracker deep Red FM probe (1:10000, Yeasen, China, 407431ES50) for 30 min at 37 °C. Subsequently, the cells were stained with a 0.1% DAPI solution (ZSGB-BIO, Beijing, China, ZLI-9557) for 5 min at 37 °C. The stained cells were then imaged using a fluorescent inverted microscope Confocal Imaging System (Leica Microsystems, Germany) with randomly selected fields of view. The mitochondrial length was analyzed using ImageJ FIJI software by Mitochondrial Network Analysis (MiNA) toolset.

Mitochondrial ROS (mROS) assay

The levels of mitochondrial ROS were detected using the fluorescent probes MitoSOX™ Green (1:1000, Thermo Fisher Scientific, USA, M36005), and fluorescent intensity was measured using a confocal microscope (Nikon, Tokyo, Japan).

Glutathione and oxidized glutathione and malondialdehyde detection

Levels of Glutathione (GSH), Oxidized glutathione (GSSG), and Malondialdehyde (MDA) in HepG2 and LO2 cells, and liver tissues from different groups were measured using the GSH/GSSG assay kit (Beyotime, Shanghai, China, S0053) and MDA assay kit (Beyotime, Shanghai, China, S0053), respectively, according to the manufacturer's instructions.

Mitochondrial membrane potential

JC-1 staining solution (Beyotime, Shanghai, China, C2003S) was used to analyze the mitochondrial membrane potential in HepG2 and LO2 cells and livers. The JC-1 probe reagent was diluted in fresh medium at a ratio of 1:1000, as recommended by the manufacturer. Subsequently, the HepG2 and LO2 cells, and liver slides were incubated with the diluted JC-1 probe in the dark at 37 °C for 20 min. After fixation with 4% paraformaldehyde, the HepG2 and LO2 cells, and liver slides were counterstained with 0.1% DAPI solution (ZSGB-BIO, Beijing, China, ZLI-9557) for 5 min at 37 °C. Images were captured using a confocal microscope (Nikon, Tokyo, Japan), and the mean fluorescent intensity was calculated using ImageJ FIJI software.

Enzyme-linked immunosorbent assay (ELISA)

Levels of ATP and ATPase activity in HepG2 and LO2 cells from different groups were measured using the enhanced ATP assay kit (Beyotime, Shanghai, China, S0027) and ATPase assay kit (Shanghai Enzyme-linked Biotechnology Co, China, ml503692), respectively, according to the manufacturer's instructions.

Oxygen consumption rate (OCR)

HepG2 and LO2 cells were grown in 96-well plates and treated with the designated treatments. Extracellular OCR was performed following the instructions provided with the extracellular OCR plate assay kit (Dojindo, Japan, E297). The phosphorescence intensity was measured using a multifunctional enzyme marking instrument (Thermo Fisher Scientific, USA, Varioskan LUX multimode microplate reader).

Nile red staining

The cultured cells were fixed with 4% paraformaldehyde for 30 min. After fixation, Nile red at a concentration of 0.5 μg/mL (Sigma, USA, 72485) was added to the cells for 5 min to visualize lipid droplets. The nucleus was stained with a 0.1% DAPI solution (ZSGB-BIO, Beijing, China, ZLI-9557) for 5 min. The fluorescence was captured using the CytationTM5 instrument (BioTek, USA) and quantified using ImageJ FIJI software.

MSC-sEV injection and tracking

C57BL/6 mice (female, 19 ± 1 g) were used to establish the high-fat diet (HFD, 45% of calories from fat) model as described [31]. All animals were kept on a 12-hour light/12-hour dark cycle at a temperature of 23 ± 2 ℃ and

a relative humidity of 55 ± 5%. After acclimatization for 1 week, the experimental mice were randomly assigned to four groups: NCD group, mice received a normal chow diet (NCD) with 10% of calories from fat ($n = 6$); PBS group, HFD-fed mice treated with PBS ($n = 6$); MSC-sEV (5 mg/kg) group, HFD-fed mice treated with 5 mg/kg MSC-sEV ($n = 6$); MSC-sEV (10 mg/kg) group, HFD-fed mice treated with 10 mg/kg MSC-sEV ($n = 6$). Mice were fed a high-fat diet for 10 weeks and then injected with MSC-sEV (*i.v.*) or equivalent volumes of PBS (*i.v.*) for 4 weeks. Additionally, the MSC-sEV was labeled using Dir (Sigma-Aldrich, USA) according to the manufacturer's instructions. To track MSC-ex in mice, we intravenously injected 1.2×10^9 labeled MSC-sEV and analyzed using a Maestro in vivo imaging system (CRI, Massachusetts, USA). Spectral imaging at 690–850 nm was performed in vivo 24 h after injection with an exposure time of 150 ms/image. At the end of the study, all animals were anesthetized using isoflurane inhalation (2%, 0.5 L/min), and blood samples and livers were collected for further analysis. The work has been reported in line with the ARRIVE guidelines 2.0.

Immunofluorescence

For immunofluorescence analyses, HepG2 cells and liver sections were treated with 4% paraformaldehyde for 30 min and permeabilized using 0.1% Triton X-100 for 30 min. After blocking with 5% BSA for 60 min, the cells and liver sections were incubated with antibodies at 4 °C for 12 h. They were stained with corresponding isotype-specific secondary antibodies for 1 h in the dark. Nuclei were stained with a 0.1% DAPI solution (ZSGB-BIO, Beijing, China, ZLI-9557), and the images were obtained using a fluorescent inverted microscope Confocal Imaging System (Leica Microsystems, Germany). The primary antibodies used were CD9 (1:200, Bioworld, USA, BS3022), RNF31 (1:200, Bioworld, USA, BS71127), and DRP1 (1:200, ABclonal, Wuhan, China, A2586).

Immunohistochemistry

The embedded liver sections in paraffin were dewaxed and rehydrated. Further antigen reparative process was performed, and the endogenous peroxidase was rendered inactive with a 3% hydrogen peroxide (H_2O_2) solution for 30 min. A 5% BSA blocking solution was applied before incubating with the primary antibody. Subsequently, the slides were incubated with the secondary antibody at room temperature for 1 h. Finally, the slides were stained with hematoxylin. Images were captured using an Olympus microscopy CX41 (Tokyo, Japan). The primary antibodies used were DRP1 (1:100, ABclonal, Wuhan, China, A2586).

Hematoxylin and Eosin (H&E) staining

The livers were rinsed with PBS and fixed with 4% paraformaldehyde. The tissues were then embedded in paraffin and sliced into 4 μm thick sections. To observe the histological damage in the liver sections, the slides were treated with xylene to remove the paraffin, followed by rehydration using various ethanol solutions. Finally, the slides were stained with H&E staining to evaluate the tissue structure under the microscope (Leica Microsystems, Germany).

Oil red staining

Fresh livers were preserved by freezing them at optimal cutting temperatures and then cut into frozen sections. The slides were fixed with 4% paraformaldehyde for 30 min and subsequently stained with Oil Red O (Sigma, USA, O0625) following the manufacturer's instructions. Randomly selected oil droplet images were observed under a fluorescence microscope (Leica Microsystems, Germany), and the images were analyzed using ImageJ FIJI software.

Quantitative reverse transcription-PCR (qRT-PCR)

RNA samples were acquired from liver tissues using Trizol (Invitrogen, USA, 15596026CN) as per the manufacturer's guidelines. The cDNA was generated using the SuperScript Reverse Transcriptase Kit (Vazyme, Nanjing, China, Q511-02), and the qRT-PCR experiment was performed using SYBR green (CWBIO, Beijing, China, CW0659). The relative gene expression, which was adjusted for β-actin, was determined using the $2^{-\Delta\Delta Ct}$ technique. There were six replicates for each group. The primers were listed in the Table. S1.

Liquid chromatography-tandem MS analysis of MSC-sEV

Mass spectrometry analysis of small extracellular vesicles (sEV)-associated proteins was studied using LC-MS/MS. Briefly, the MSC-sEV solution was sonicated before the protein contents were extracted. Afterward, 1 M dithiothreitol and 1 M iodoacetamide were included to reduce and alkylate the extracted proteins. The samples were then digested using 20 ng/μL trypsin overnight at 37 ˚C. Next, the mixtures were centrifuged at 12,010 rpm for 20 min. Then, the filtrate was collected and dried at 55 ˚C to obtain the polypeptides. The dried polypeptide samples were reconstituted in 0.1% aqueous formic acid and desalted via ZipTip C18 columns (Thermo Fisher Scientific, USA). The samples were recovered from the columns with water containing 2% acetonitrile and 0.1% formic acid. Finally, the samples were analyzed with Nano Liquid Chromatography–Orbitrap Mass Spectrometry (Easy-nLC1200, Q-Exactive Plus, Thermo Fisher Scientific, USA). Proteins identified by MS were annotated and analyzed using PANTHER software (Protein Analysis

Through Evolutionary Relationships; http://www.pantherdb. org).

Co-immunoprecipitation (Co-IP)

To investigate the interaction among RNF31, DRP1, and FIS1, we performed a Co-IP assay using a Pierce Classic Magnetic IP/Co-IP Kit (Thermo Fisher, USA) following the manufacturer's protocol. Briefly, the cell lysates were incubated with primary antibodies and washed with NaCl buffer. Subsequently, the samples were boiled for 10 min in 2 × SDS loading buffer before being collected for western blotting. The antibodies used in this study were as follows: RNF31 (1:1000, Bioworld, USA, BS71127), DRP1 (1:4000, ABclonal, Wuhan, China, A2586) and FIS1 (1:1000, ABclonal, Wuhan, China, A5821).

Plasmid and siRNA transfection

The pRNF31 expression vectors (pCDNA3.1-RNF31) were constructed using the full-length human RNF31 cDNA (NM_001310332.2). Small interfering RNA (siRNA) targeting RNF31 and control scrambled siRNA were designed by Genepharma, Suzhou, China. The fragments were mixed with Lipofectamine 2000 (Thermo Fisher Scientific, Waltham, MA, USA) in a solution of Opti-MEM (Gibco, Carlsbad, CA, USA). After incubation for 20 min, the solution was added to the cell medium. Cell protein or RNA samples were harvested 48 h after transfection.

Lentiviral knockdown of RNF31 in MSCs and preparation of MSC-sEVshRNF31

The lentiviral vector (pLKO.1-GFP-Puro-shRNF31; Vigen Biotech, Shanghai, China) was explicitly designed to target RNF31 silencing. A negative control vector (pLKO.1-Puro-shRNA) was also prepared. RNF31 shRNA (sequence: GCT GCA GCT TTC AGA ATT TGA) and control shRNA (non-targeting) oligonucleotides were inserted into the pLKO.2-U6-MSC-hPGK-cop-GFP -puro lentiviral vector to generate RNF31 and control green fluorescent protein (GFP)-labeled shRNA expression vectors. After virus preparation, MSCs were transduced with recombinant lentivirus (pLKO) (pLKO.1-GFP-Puro-shRNF31 or pLKO.1-Puro-shRNA, 25 multiplicity of infection) and selected with 1 mg/ml puromycin (Sigma, St. Louis, MO, 540411) for 2 days. Subsequently, shRNA expression in MSCs was induced with 80 μg/ml doxycycline. MSC^{shCtr} and MSC^{shRNF3} were established for the collection of MSC-sEV^{shCtr} and MSC-$sEV^{shRNF31}$.

MSC-sEVshCtr and MSC-sEVshRNF31 injection and tracking

To compare the effect of MSC-sEV^{shCtr} and MSC-$sEV^{shRNF31}$ injection on lipid deposition in HFD-fed mice. C57BL/6 female mice weighing 19 ± 1 g were randomly assigned to five groups: NCD group, mice received a normal chow diet (NCD) with 10% of calories from fat ($n = 6$); PBS group, HFD-fed mice treated with PBS ($n = 6$); MSC-sEV^{shCtr} group, HFD-fed mice treated with 10 mg/kg MSC-sEV^{shCtr} ($n = 6$); MSC-$sEV^{shRNF31}$group, HFD-fed mice treated with 10 mg/kg MSC-$sEV^{shRNF31}$ ($n = 6$); Mdivi-1 group, HFD-fed mice treated with 10 mg/kg Mdivi-1 ($n = 6$). Mice were fed the high-fat diet for 10 weeks and then injected with MSC-sEV^{shCtr} (*i.v.*), MSC-$sEV^{shRNF31}$ (*i.v.*), Mdivi-1 (MCE, USA, HY-15886, *i.p.*), or PBS (*i.v. and i.p.*) for 4 weeks. The MSC-sEV^{shCtr} and MSC-$sEV^{shRNF31}$ were labeled with Dir (Sigma-Aldrich, USA) according to the manufacturer's instructions to visualize their uptake. 1.2×10^9 labeled MSC-sEV^{shCtr} and MSC-$sEV^{shRNF31}$ were injected into the mice via the tail vein for perfusion. After 24 h, an in vivo imaging was performed to visualize the location. Body weight was monitored weekly throughout the experiment. Mice ($n = 6$ per group) were individually housed and euthanized after a 12-hour overnight fast at the end of the study. Blood samples were collected from the retinal vein plexus, centrifuged at 3,500 rpm for 10 min at 4 °C to separate the serum, and stored at − 80 °C for further analysis. The liver index (liver weight/body weight) was calculated by removing and weighing the entire liver. At the end of the study, all animals were anesthetized using isoflurane inhalation (2%, 0.5 L/min), and blood samples and livers were collected for further analysis. The work has been reported in line with the ARRIVE guidelines 2.0.

Analysis of biochemical indicators of mice serum

Levels of alanine transaminase (ALT), aspartate transaminase (AST) in mice serum were detected according to manufacturers' instructions with a MINDRAY BS200 chemistry analyzer (MINDRAY Medical International Co., Shenzhen, China).

Hepatic lipid extraction

For hepatic lipid extraction, a consistent portion of liver tissues was excised from all mouse groups. A lipid extraction reagent was prepared using chloroform, methanol, and PBS at an 8:4:3 ratio. 75 mg of liver tissues were thoroughly mixed with the extraction reagent overnight at 4 °C. After 12 h of incubation, the mixture was centrifuged at 3,000 rpm for 20 min at 4 °C. The lower organic phase was collected, samples were evaporated under nitrogen flow, and then resuspended in 200 μL methanol. The levels of liver Triglyceride (TG) and Total Cholesterol (TC) were analyzed using the MINDRAY BS200 chemistry analyzer from MINDRAY Medical International Co., Shenzhen, China, following the manufacturer's instructions.

Statistical analysis

The data were analyzed using GraphPad Prism software (version 6.0) and presented as mean ± standard deviation (SD). Students' t-tests were used to determine the statistical significance between the two groups. For studies with more than two groups, one-way analyses of variance (ANOVA) were used to analyze the data. All statistical tests were performed using a two-tailed approach, and $p < 0.05$ was considered statistically significant.

Results

MSC-sEV inhibits mitochondrial fission and reduces lipotoxic hepatocyte lipid deposition

We initially investigated the role of MSC-sEV in regulating DRP1 expression and mitochondrial fission processes in hepatocytes. Western blot analysis confirmed the presence of extracellular vesicle marker proteins, including CD9, CD63, and TSG101. In contrast, the endoplasmic reticulum membrane protein Calnexin was not detected (Fig. 1a). The size distribution and morphologies of MSC-sEV were examined using NTA and TEM (Fig. 1b). To assess the direct impact of MSC-sEV on mitochondrial fission, HepG2 cells and human hepatocyte LO2 cells were treated with 1.0 mM OPA to induce lipotoxic injury (Additional file 4: Fig. S1a). The results demonstrated that MSC-sEV labeled with the fluorescent dye Dir were internalized by HepG2 and LO2 cells in normal or lipotoxic conditions (Fig. 1c, Additional file 4: Fig. S1b). The protein expression of mitochondrial fission protein DRP1 remained consistent in normal HepG2 and LO2 cells following treatment with MSC-sEV (Fig. 1d, Additional file 4: Fig. S1c). When compared to cells treated with PBS and MSC culture medium depleted of sEV (de-MSC-sEV), the protein expression of DRP1 in lipotoxic HepG2 and LO2 cells treated with MSC-sEV were significantly reduced (Fig. 1e, Additional file 4: Fig. S1d). MitoTracker Red staining revealed that lipotoxic HepG2 and LO2 cells in the PBS group exhibited fragmented and shorter mitochondria, whereas the MSC-sEV group displayed networked and longer mitochondria (Fig. 1f, Additional file 4: Fig. S1e). These findings indicate that MSC-sEV effectively inhibits mitochondrial fission in lipotoxic hepatocytes.

Abnormal mitochondrial fission can lead to mitochondrial damage, including increased mROS, decreased membrane potential, and lipid deposition in hepatocytes [32]. Our results demonstrated a reduction in levels of mROS and lipid peroxidation product MDA, as well as an increase in the levels of the antioxidant molecule GSH/GSSG ratio in hepatocytes treated with MSC-sEV (Fig. 1g-i, Additional file 4: Fig. S1f-h). Furthermore, JC-1 and Nile Red staining confirmed that MSC-sEV restored the mitochondrial membrane potential of lipotoxic hepatocytes and inhibited lipid deposition (Fig. 1j, k, Additional file 4: Fig. S1i, j). These findings suggest that MSC-sEV can inhibit DRP1 expression in lipotoxic hepatocytes, suppress mitochondrial fission, alleviate hepatocyte oxidative stress and mitochondrial damage, and reduce hepatocyte lipid deposition.

MSC-sEV inhibits DRP1 expression and mitigates mitochondrial damage in HFD-fed mice's liver tissues

We then investigated the inhibitory effect of MSC-sEV on DRP1 expression and mitochondrial fission in HFD-fed mice. The HFD-diet significantly promoted the deposition of lipid in the liver of MASLD mice at 10 weeks compared to the NCD-diet (Additional file 4: Fig. S2a). After 10 weeks of HFD feeding, PBS or MSC-sEV (5 mg/kg or 10 mg/kg body weight) were injected into HFD-fed mice through the tail vein. In vivo, imaging of Dir labeled MSC-sEV and immunofluorescence of MSC-sEV marker CD9 confirmed that MSC-sEV primarily accumulated in the liver (Fig. 2a, b, Additional file 4: Fig. S2b). The expression of DRP1 was reduced in the livers of HFD-fed mice in the MSC-sEV group compared to the PBS group, as observed through western blot and immunohistochemistry analysis (Fig. 2c, d). Moreover, MSC-sEV injection reduced serum aspartate transaminase (AST) (Fig. 2e), serum alanine transaminase (ALT) (Fig. 2f), liver triglyceride (TG) (Fig. 2g), and liver total cholesterol (TC) (Fig. 2h). Additionally, MSC-sEV injection also resulted in decreased levels of mROS and MDA in the liver tissue, along with increased levels of the antioxidant molecule GSH/GSSG ratio (Fig. 2i-k, Additional file 4: Fig. S2c). Results of JC-1 staining demonstrated impaired mitochondrial membrane potential in the livers of HFD-fed mice, while MSC-sEV treatment improved the damaged mitochondrial membrane potential in liver tissue cells (Fig. 2l, Additional file 4: Fig. S2d). H&E and Oil Red O staining revealed significant vacuolar degeneration and lipid deposition in the liver tissue of mice on the HFD diet for 14 weeks (Fig. 2m, n, Additional file 4: Fig. S2e). In contrast, the livers of the MSC-sEV group exhibited a more intact structure with lower lipid deposition and less inflammation (Fig. 2m-o). These findings indicate that MSC-sEV injection effectively suppresses DRP1 expression, reduces oxidative stress and mitochondrial damage in liver tissue, and alleviates lipid deposition and associated liver damage.

MSC-sEV delivered RNF31 down-regulates DRP1 expression in lipotoxic hepatocytes and liver tissue of HFD-fed mice

To explore which MSC-sEV components confer mitochondrial fission inhibition effects, we analyzed the protein profile in MSC-sEV using LC-MS/MS. E3 ubiquitin ligase plays a critical role in mitochondrial fission and the maintenance of mitochondrial homeostasis [33]. We

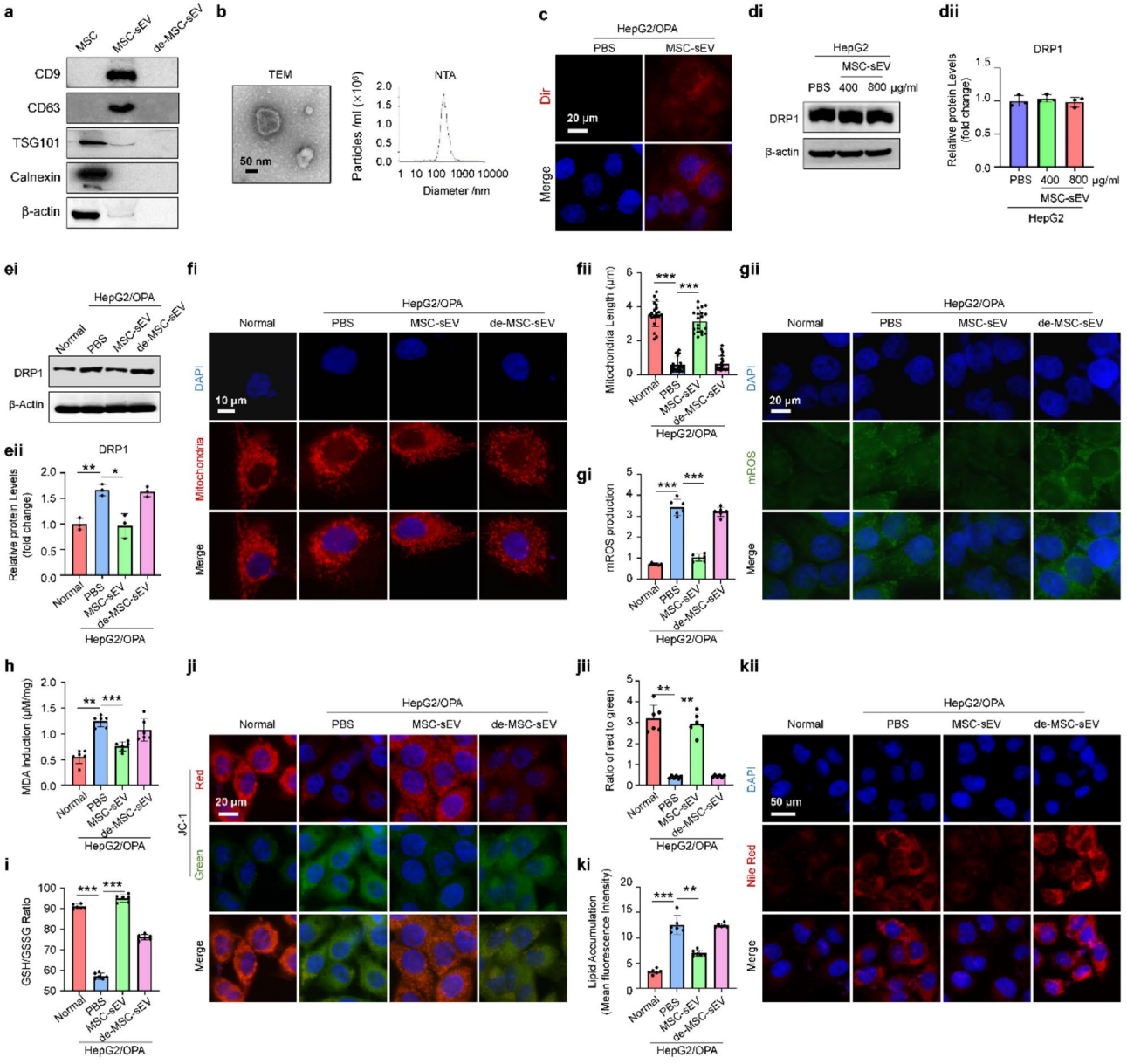

Fig. 1 MSC-sEV inhibits mitochondrial fission and reduces lipotoxic hepatocytes lipid deposition. **a** Western blot analysis of exosomal markers CD9, CD63, TSG101, and Calnexin in MSC, MSC-sEV, and MSC-sEV-free conditional medium (de-MSC-sEV). (Full-length blots are presented in Additional file 1, Fig.S1). **b** Nanoparticle tracking analysis (NTA) and Transmission Electron Microscope (TEM) analysis of MSC-sEV. Scale bar, 20 nm. **c** Uptake of Dir labeled MSC-sEV by OPA injured HepG2 cells. Scale bar, 50 μm. **d** Western blot analysis of DRP1 protein expression in normal HepG2 cells treated with PBS, MSC-sEV (400 μg/mL and 800 μg/mL). ($n=3$). (Full-length blots are presented in Additional file 1, Fig.S2). **e** Western blot analysis of DRP1 protein expression in normal HepG2 cells and OPA-injured HepG2 cells treated with PBS, MSC-sEV (800 μg/mL), and de-MSC-sEV. ($n=3$; * $P<0.05$, ** $P<0.01$). (Full-length blots are presented in Additional file 1, Fig.S3). **f** MitoTracker Deep Red staining and mitochondria length statistics in normal HepG2 cells and OPA injured HepG2 cells treated with PBS, MSC-sEV (800 μg/mL), and de-MSC-sEV. Scale bar, 10 μm. ($n=20$; *** $P<0.001$). **g** Mitochondrial reactive oxygen species (mROS) production in normal HepG2 cells and OPA-injured HepG2 cells treated with PBS, MSC-sEV (800 μg/mL), and de-MSC-sEV. Scale bar, 20 μm. ($n=6$; *** $P<0.001$). **h**, **i** Malondialdehyde (MDA) induction and Glutathione (GSH)/Oxidized glutathione (GSSG) ratio in normal HepG2 cells and OPA-injured HepG2 cells treated with PBS, MSC-sEV (800 μg/mL), and de-MSC-sEV. ($n=6$; ** $P<0.01$, *** $P<0.001$). **j** JC-1 staining of mitochondria membrane potential in normal HepG2 cells and OPA-injured HepG2 cells treated with PBS, MSC-sEV (800 μg/mL), and de-MSC-sEV. Scale bar, 20 μm. ($n=6$; ** $P<0.01$). **k** Nile red staining of intracellular lipid droplets in normal HepG2 cells and OPA-injured HepG2 cells treated with PBS, MSC-sEV (800 μg/mL), and de-MSC-sEV and quantified by ImageJ FIJI software. Scale bars, 50 μm. ($n=6$; ** $P<0.01$, *** $P<0.001$)

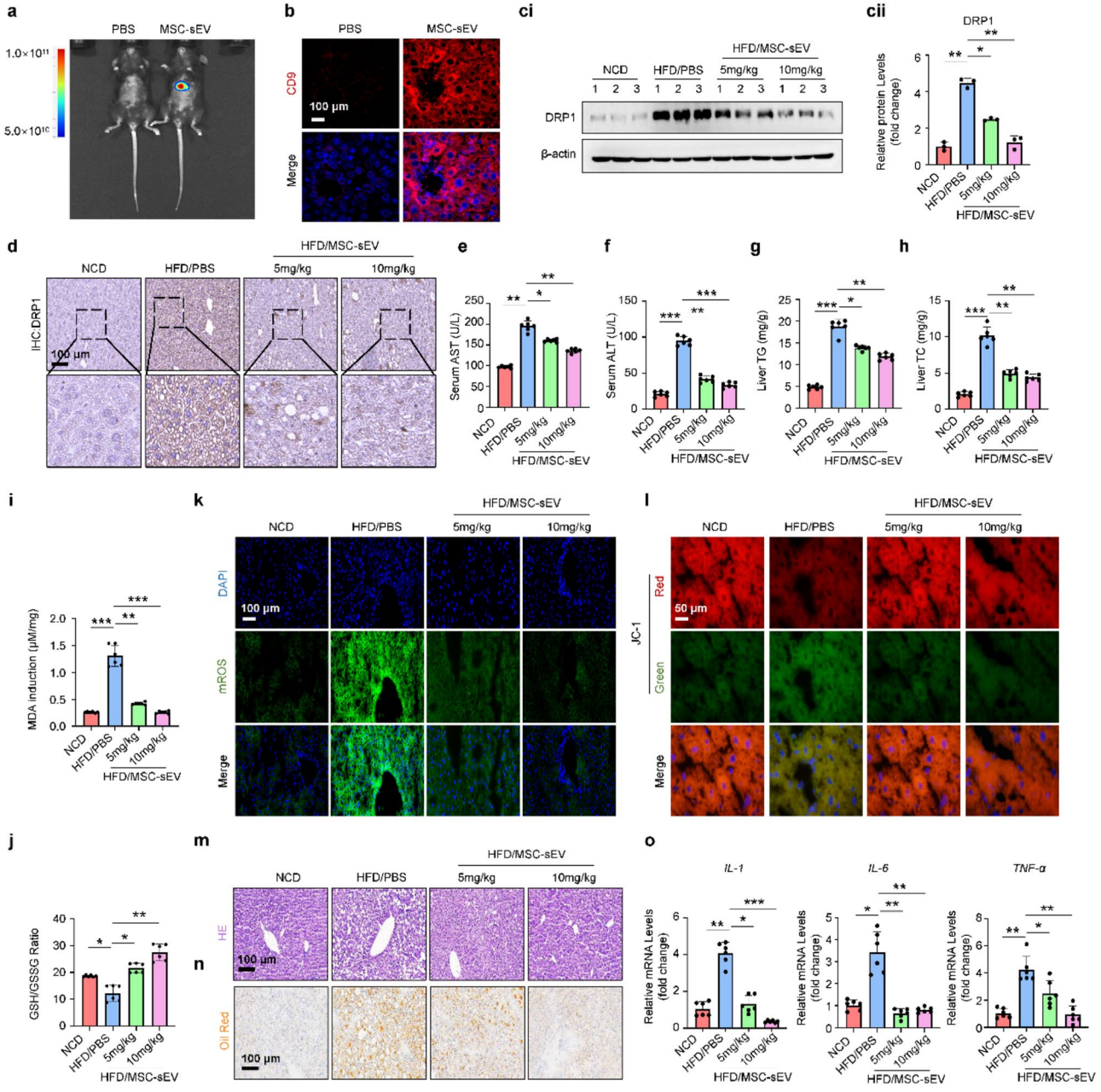

Fig. 2 **MSC-**sEV inhibits DRP1 expression and mitigates mitochondrial damage in HFD-fed mice's livers. **a** Biodistribution of MSC-sEV in HFD-fed mice after MSC-sEV *i.v.* injection for 24 h. **b** Immunofluorescence analysis of human CD9 protein in HFD-fed mice livers after MSC-sEV *i.v.* injection. Scale bar, 100 μm. **c** Western blot analysis of DRP1 protein expression in livers from normal chow diet (NCD) fed mice, HFD-fed mice treated with PBS or MSC-sEV. ($n = 3$; * $P < 0.05$, ** $P < 0.01$). (Full-length blots are presented in Additional file 1, Fig.S4). **d** Immunohistochemistry analysis of DRP1 protein in livers from normal chow diet (NCD) fed mice, HFD-fed mice treated with PBS or MSC-sEV. Scale bar, 100 μm. **e**, **f** Serum AST and ALT levels from normal chow diet (NCD) fed mice, HFD-fed mice treated with PBS or MSC-sEV. ($n = 6$; * $P < 0.05$; ** $P < 0.01$, *** $P < 0.001$). **g**, **h** Liver TG (mg/g) and TC (mg/g) levels from normal chow diet (NCD) fed mice, HFD-fed mice treated with PBS or MSC-sEV. ($n = 6$; * $P < 0.05$; ** $P < 0.01$, *** $P < 0.001$). **i**, **j** MDA induction and GSH/GSSG ratio in livers from normal chow diet (NCD) fed mice and HFD-fed mice treated with PBS or MSC-sEV. ($n = 6$; * $P < 0.05$, ** $P < 0.01$, *** $P < 0.001$). **k** mROS production in livers from normal chow diet (NCD) fed mice, HFD-fed mice treated with PBS or MSC-sEV. Scale bar, 100 μm. **l** JC-1 staining of mitochondria membrane potential in livers from normal chow diet (NCD) fed mice, HFD-fed mice treated with PBS or MSC-sEV. Scale bar, 50 μm. **m**, **n** H&E and Oil red O staining in livers from normal chow diet (NCD) fed mice, HFD-fed mice treated with PBS or MSC-sEV. Scale bars, 100 μm. **o** Relative mRNA expression of IL-1, IL-6 and TNF-α in livers from normal chow diet (NCD) fed mice, HFD-fed mice treated with PBS or MSC-sEV ($n = 6$; * $P < 0.05$, ** $P < 0.01$, *** $P < 0.001$)

found that RNF31 (also called HOIP), UBC and TRAF7 proteins were listed in the proteins involved in ubiquitination processes (Fig. 3a, b). Researches have indicated that the impairment of RNF31 plays a crucial role in hepatocyte inflammation and apoptosis, ultimately contributing to the development of non-alcoholic steatohepatitis and cirrhosis [34–36]. Our hypothesis suggests that RNF31 serves as a key active component in MSC-sEV, working to suppress mitochondrial fission and lipid accumulation. Western blot analysis confirmed the expression of RNF31 protein in MSC and MSC-sEV (Fig. 3c). RNF31 protein level was significantly increased in lipotoxic HepG2 and LO2 cells treated with MSC-sEV but not de-MSC-sEV (Fig. 3d, Additional file 4: Fig. S3a). Immunofluorescence analysis demonstrated co-localization between RNF31 and CD9 in MSC-sEV treated lipotoxic HepG2 cells (Fig. 3e). RNF31 protein level was also increased by MSC-sEV in livers of HFD-fed mice (Fig. 3f, g). In normal HepG2 and LO2 cells, the expression of RNF31 was only weakly affected by MSC-sEV treatment (Additional file 4: Fig. S3b, c). Furthermore, treatment with MSC-sEV did not induce changes of UBC and TRAF7 proteins in lipotoxic HepG2 and LO2 cells (Additional file 4: Fig. S3d, e).

DRP1 is a crucial factor in the regulation of mitochondrial fission [37]. We found that the expression of RNF31 decreased in hepatocytes while the expression of DRP1 increased at 24 h post OPA treatment (Fig. 3h). Result of Co-IP also showed that RNF31 interacted with DRP1, but not with FIS1 in HepG2 cells (Fig. 3i). RNF31 may be related to regulating DRP1 expression in lipotoxic hepatocytes. To further understand the effect of RNF31 on DRP1 expression, we demonstrated that RNF31 overexpression inhibited the protein expression of DRP1 in OPA-injured HepG2 and LO2 cells (Fig. 3j, Additional file 4: Fig. S3f). And the knockdown of RNF31 promoted the protein expression of DRP1 in normal HepG2 and LO2 cells (Fig. 3k, Additional file 4: Fig. S3g). Therefore, MSC-sEV may transfer RNF31 protein to reduce mitochondrial fission and DRP1 expression in lipotoxic HepG2 and LO2 cells.

RNF31 inhibits mitochondrial fission and reduces lipid deposition in lipotoxic hepatocytes

We further investigated the inhibitory effects of RNF31 on oxidative stress, mitochondrial damage, and lipid deposition in lipotoxic hepatocytes. OPA-injured HepG2 cells were transfected with the pCtr or pRNF31 plasmid. The results revealed that overexpression of RNF31 led to increased cellular mitochondrial network and mitochondrial length observed by MitoTracker Red staining (Fig. 4a, Additional file 4: Fig. S4). Besides, overexpression of RNF31 in lipotoxic HepG2 cells can also contribute to a reduction in the levels of mROS and MDA (Fig. 4b, c, Additional file 4: Fig. S4b), while an increase in the levels of GSH/GSSG ratio in lipotoxic HepG2 cells (Fig. 4d). Furthermore, the overexpression of RNF31 rescued mitochondrial function, evidenced by elevated levels of mitochondrial membrane potential (Fig. 4e, Additional file 4: Fig. S4c), ATP content (Fig. 4f), ATPase activity (Fig. 4g), and mitochondrial oxygen consumption rate (OCR) (Fig. 4h). Additionally, RNF31 overexpression led to a decrease in lipid deposition in lipotoxic HepG2 cells (Fig. 4i). To further confirm the role of RNF31, we used RNF31 siRNA transfection to knock down RNF31 expression in normal HepG2 cells. The knockdown of RNF31 reduced the mitochondrial network, and mitochondrial length (Fig. 4j, Additional file 4: Fig. S4d). Consistently, the knockdown of RNF31 increased the levels of mROS and MDA (Fig. 4k, l, Additional file 4: Fig. S4e), while decreasing the GSH/GSSG ratio content in normal HepG2 cells compared to the siCtr transfection group (Fig. 4m). Moreover, the knockdown of RNF31 resulted in reduced mitochondrial membrane potential, ATP content, ATPase activity, and OCR combined with the increased lipid deposition in hepatocytes (Fig. 4n-r, Additional file 4: Fig. S4f). These findings indicate that RNF31 is crucial in inhibiting mitochondrial fission, improving mitochondrial function and reducing hepatocyte lipid deposition.

DRP1 inhibition reverses the promotion effect of RNF31 knockdown on mitochondrial fission and lipid deposition

To further confirm the role of DRP1 in RNF31-regulated hepatocyte mitochondrial fission, we investigated the impact of Mdivi-1, a DRP1 inhibitor, on hepatocyte mitochondrial fission and lipid deposition that were increased by RNF31 siRNA. Western blot analysis demonstrated that Mdivi-1 diminished the high level of protein expression of DRP1 caused by RNF31 knockdown in normal HepG2 and LO2 cells (Fig. 5a, Additional file 4: Fig. S5a). MitoTracker Red staining revealed that compared to the siCtr group, the mitochondria of normal HepG2 cells in the siRNF31/PBS group appeared shorter and more fragmented. In contrast, the mitochondria of cells in the siRNF31/Mdivi-1 group appeared longer and less fragmented (Fig. 5b). Moreover, Mdivi-1 reversed the increase in mROS and MDA levels and the decrease in GSH/GSSG ratio in normal HepG2 cells caused by RNF31 knockdown (Fig. 5c-e). Furthermore, the mitochondrial membrane potential, ATP content, ATPase activity and OCR increased in the siRNF31/Mdivi-1 group, while lipid deposition decreased compared to the siRNF31/PBS group, indicating that Mdivi-1 can alleviate the mitochondrial damage and lipid deposition in hepatocytes caused by RNF31 knockdown (Fig. 5f-j, Additional file 4: Fig. S5b). These findings suggest that inhibiting DRP1 can reverse the regulatory effect of

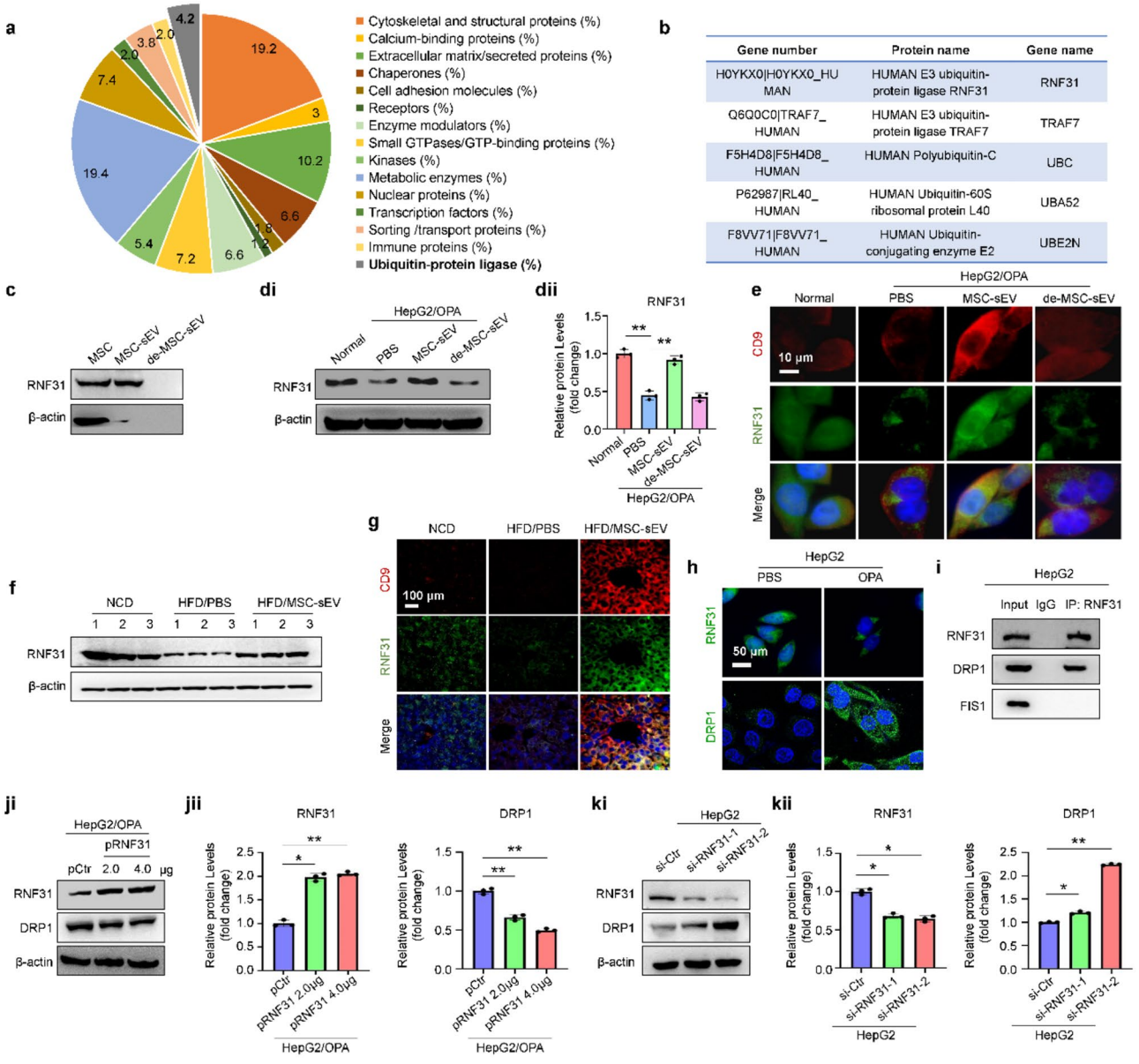

Fig. 3 MSC-sEV delivered RNF31 down-regulates DRP1 expression in lipotoxic hepatocytes and livers of HFD-fed mice. **a** Proteomic profiling and protein classification diagram of MSC-sEV by LC-MS/MS. **b** A partial list of proteins involved in ubiquitination processes. **c** Western blot analysis of RNF31 protein expression in MSC, MSC-sEV and MSC-sEV-free conditional medium supernatant (de-MSC-sEV). (Full-length blots are presented in Additional file 1, Fig.S5). **d** Western blot analysis of RNF31 protein level in normal HepG2 cells and OPA-injured HepG2 cells treated with PBS, MSC-sEV (800 μg/mL), and de-MSC-sEV for 24 h. ($n=3$; ** $P<0.01$). (Full-length blots are presented in Additional file 1, Fig.S6). **e** CD9 (red) and RNF31 (green) co-localization were analyzed by immunofluorescence in normal HepG2 cells and OPA-injured HepG2 cells treated with PBS, MSC-sEV (800 μg/mL), and de-MSC-sEV for 24 h. Scale bar, 10 μm. **f** Western blot analysis of RNF31 protein expression in livers from normal chow diet (NCD) fed mice, HFD-fed mice treated with PBS or 10 mg/kg MSC-sEV. (Full-length blots are presented in Additional file 1, Fig.S7). **g** CD9 (red) and RNF31 (green) co-localization were analyzed by immunofluorescence in livers from normal chow diet (NCD) fed mice, HFD-fed mice treated with PBS or 10 mg/kg MSC-sEV. Scale bar, 100 μm. **h** Immunofluorescence analysis of RNF31 and DRP1 protein expression in OPA-injured HepG2 cells. Scale bar, 50 μm. **i** The interaction among RNF31, DRP1, and FIS1 detected by Co-IP assay in HepG2 cells. (Full-length blots are presented in Additional file 1, Fig.S8). **j** Western blot analysis of RNF31 and DRP1 expression in OPA injured HepG2 cells transfected with control plasmid (pCtr) or pCDNA3.1-RNF31 plasmid (pRNF31, 2.0 μg and 4.0 μg). ($n=3$; * $P<0.05$, ** $P<0.01$). (Full-length blots are presented in Additional file 1, Fig.S9). **k** Western blot analysis of RNF31 and DRP1 expression in normal HepG2 cells transfected with control siRNA (siCtr) or RNF31 siRNA. ($n=3$; * $P<0.05$, ** $P<0.01$). (Full-length blots are presented in Additional file 1, Fig.S10)

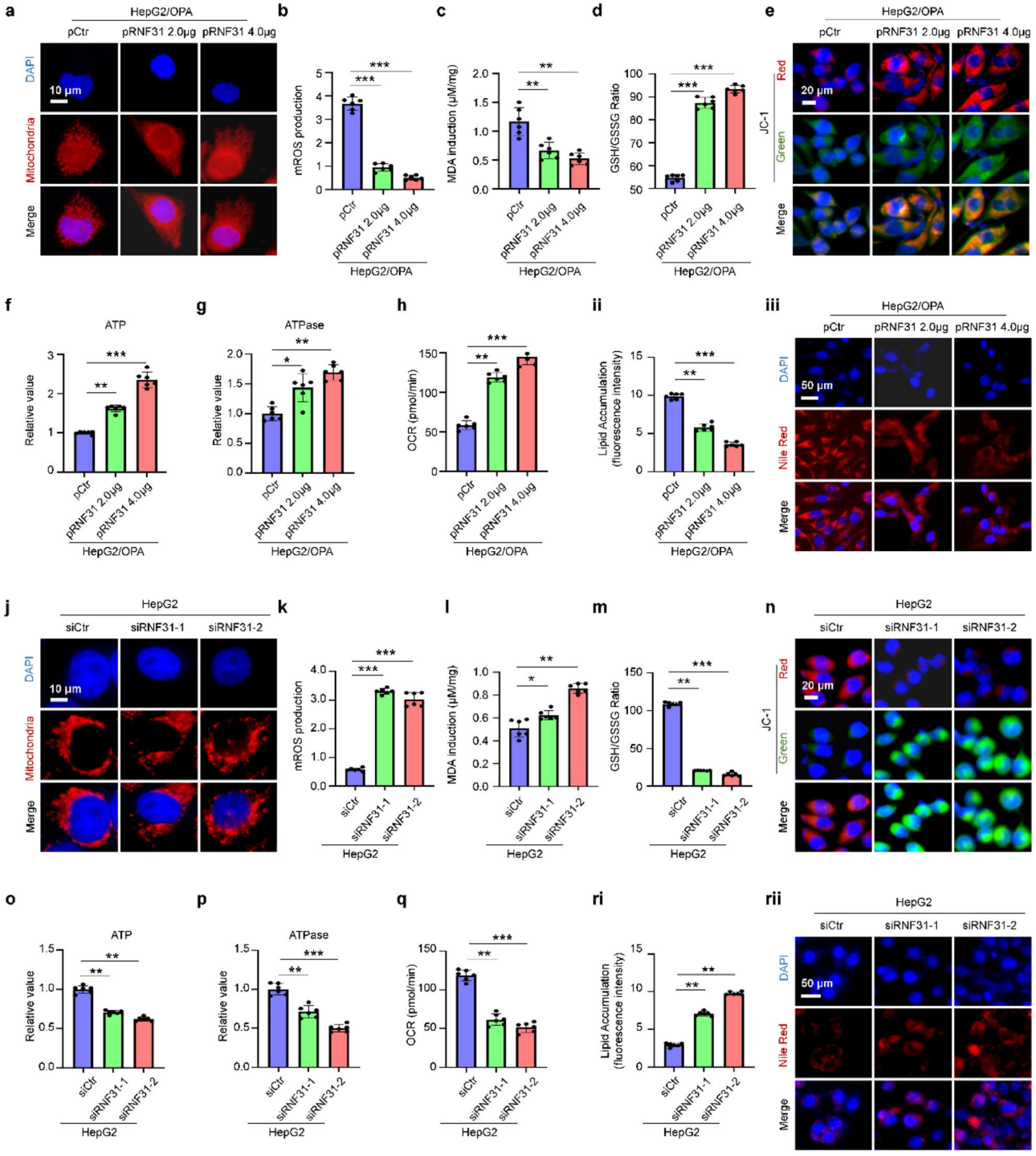

Fig. 4 (See legend on next page.)

RNF31 knockdown on mitochondrial fission and highlight the crucial role of DRP1 in RNF31-regulated mitochondrial fission and lipid deposition in hepatocytes.

RNF31 knockdown reduces the inhibitory effects of MSC-sEV on mitochondrial fission and lipid deposition in lipotoxic hepatocytes

To investigate the role of RNF31 in inhibiting hepatocyte mitochondrial fission and lipid deposition by MSC-sEV, we constructed RNF31 knockdown MSC-sEV (MSC-sEV^{shRNF31}). We compared its effects on lipotoxic

(See figure on previous page.)

Fig. 4 Overexpression of RNF31 inhibits mitochondrial fission, oxidative stress and lipid deposition in lipotoxic hepatocytes, while knockdown of RNF31 increases mitochondrial fission, oxidative stress, and lipid deposition in normal hepatocytes. **a** MitoTracker Deep Red staining and mitochondria length statistics in OPA-injured HepG2 cells transfected with the pCtr or pRNF31 (2.0 μg and 4.0 μg). Scale bar, 10 μm. **b-d** mROS production, MDA induction, and GSH/GSSG ratio in OPA-injured HepG2 cells transfected with the control plasmid (pCtr) or pRNF31 (2.0 μg and 4.0 μg). ($n=6$; ** $P<0.01$, *** $P<0.001$). **e** JC-1 staining of mitochondria membrane potential in OPA injured HepG2 cells transfected with pCtr or pRNF31. Scale bar, 20 μm. **f-h** The ATP content, ATPase activity, and OCR were measured in OPA-injured HepG2 cells transfected with the control plasmid (pCtr) or pRNF31 (2.0 μg and 4.0 μg). ($n=6$; * $P<0.05$, ** $P<0.01$, *** $P<0.001$). **i** Nile red staining of intracellular lipid droplets in OPA-injured HepG2 cells transfected with pCtr or pRNF31. Scale bar, 50 μm. ($n=6$; ** $P<0.01$, *** $P<0.001$). **j** MitoTracker Deep Red staining and mitochondria length statistics in HepG2 cells transfected with siCtr or RNF31 siRNA. Scale bar, 10 μm. **k-m** mROS production, MDA induction, and GSH/GSSG ratio in normal HepG2 cells transfected with siCtr or RNF31 siRNA. ($n=6$; * $P<0.05$, ** $P<0.01$, *** $P<0.001$). **n** JC-1 staining of Mitochondria membrane potential in normal HepG2 cells transfected with siCtr or RNF31 siRNA. Scale bar, 20 μm. **o-q** The ATP content, ATPase activity, and OCR were measured in normal HepG2 cells transfected with siCtr or RNF31 siRNA. ($n=6$; ** $P<0.01$, *** $P<0.001$). **r** Nile red staining of intracellular lipid droplets in normal HepG2 cells transfected with siCtr or RNF31 siRNA. Scale bar, 50 μm. ($n=6$; ** $P<0.01$)

hepatocytes with MSC-sEV^{shCtr}. Western blot analysis revealed a significant decrease in RNF31 protein expression in MSC^{shRNF31} and MSC-sEV^{shRNF31} compared to MSC^{shCtr} and MSC-sEV^{shCtr} (Fig. 6a). Furthermore, MSC-sEV^{shRNF31} showed a reduced ability to downregulate the protein expression of DRP1 in lipotoxic HepG2 and LO2 cells compared to MSC-sEV^{shCtr} (Fig. 6b, Additional file 4: Fig. S7a). MitoTracker Red staining revealed that compared to the PBS group, the mitochondria of lipotoxic HepG2 and LO2 cells in the MSC-sEV^{shRNF31} group appeared shorter and more fragmented. In contrast, the mitochondria of cells in the MSC-sEV^{shCtr} group appeared longer and less fragmented (Fig. 6c, Additional file 4: Fig. S7b). The detection of mROS, MDA, and GSH/GSSG ratio in lipotoxic HepG2 and LO2 cells also demonstrated that MSC-sEV^{shRNF31} treatment resulted in increased mROS and MDA levels, along with decreased GSH contents compared to MSC-sEV^{shCtr} (Fig. 6d-f, Additional file 4: Fig. S7c-e). JC-1, ATP content, ATPase activity, and OCR detection results revealed that the promotion of mitochondrial membrane potential and the improvement of lipid deposition in MSC-sEV^{shCtr} group than those in MSC-sEV^{shRNF31} group (Fig. 6g-k, Additional file 4: Fig. S6a, Fig. S7f-j). These findings suggest that the inhibitory effects of MSC-sEV on hepatocyte mitochondrial damage and lipid deposition are decreased following RNF31 knockdown.

RNF31 knockdown diminishes the role of MSC-sEV on mROS production and lipid deposition in HFD-fed mice

The effect of RNF31 on hepatocyte lipid deposition was also analyzed in HFD-fed mice injected with MSC-sEV^{shCtr} and MSC-sEV^{shRNF31}. C57BL/6 mice given an HFD (45%) for 10 weeks were given intravenous injections of either PBS or 10 mg/kg of MSC-sEV^{shCtr} or 10 mg/kg of MSC-sEV^{shRNF31}. In vivo imaging demonstrated that 24 h post-injection, MSC-sEV^{shCtr} and MSC-sEV^{shRNF31}, tagged with Dir fluorescent dye, were able to be precisely located inside the liver tissue (Fig. 7a, b). Interestingly, we also found that the effect of MSC-sEV^{shCtr}-mediated promotion in the liver index (Fig. 7c) and reduction in body weight (Fig. 7d), serum AST (Fig. 7e), serum ALT (Fig. 7f), liver TG (Fig. 7g), and liver TC (Fig. 7h) were diminished by RNF31 knockdown in MSC-sEV^{shCtr}.

Compared with the PBS group, the liver mROS and MDA levels of MSC-sEV^{shCtr}-injected mice were reduced, and the GSH/GSSG ratio and mitochondrial membrane potential were increased, indicating a similar oxidative stress inhibition as the DRP1 inhibitor Mdivi-1 (Fig. 7i-l, Additional file 4: Fig. S8a). MSC-sEV^{shRNF31}-injected mice, on the other hand, exhibited increased mROS and MDA levels in liver tissue and decreased GSH/GSSG ratio and mitochondrial membrane potential (Fig. 7i-l, Additional file 4: Fig. S8a). H&E and DRP1 immunohistochemical staining also demonstrated that MSC-sEV^{shRNF31} failed to reduce DRP1 expression and inhibited hepatocyte degeneration (Fig. 7m). Oil Red staining results revealed that while MSC-sEV^{shCtr} and Mdivi-1 significantly inhibited lipid deposition and inflammation in liver tissue, the inhibitory effect of MSC-sEV^{shRNF31} on lipid deposition was reduced (Fig. 7m, n, Additional file 4: Fig. S8b). These findings suggest that RNF31 knockdown diminishes the inhibitory impact of MSC-sEV^{shCtr} on hepatocyte mROS production and lipid deposition. Thus, RNF31 is identified as the key active component of MSC-sEV in inhibiting mitochondrial fission and lipid deposition in hepatocytes and repairing HFD-induced liver damage. MSC-sEV transported RNF31 inhibits lipotoxic hepatocyte mitochondrial fission and promotes hepatocyte lipid deposition by downregulating DRP1 expression.

Discussion

MSC-sEV is a potential new treatment for various liver diseases, including viral hepatitis, liver fibrosis, and MASLD [20]. However, the specific mechanism by which MSC-sEV repairs chronic liver diseases like MASLD is still unclear. DRP1 plays a crucial role in mediating damage-induced mitochondrial fission and promoting the progression of MASLD [38]. Inhibition of DRP1 in hepatocytes has been shown to prevent hepatic steatosis induced by a high-fat diet in mice [39]. This study discovered that MSC-sEV can inhibit the expression of

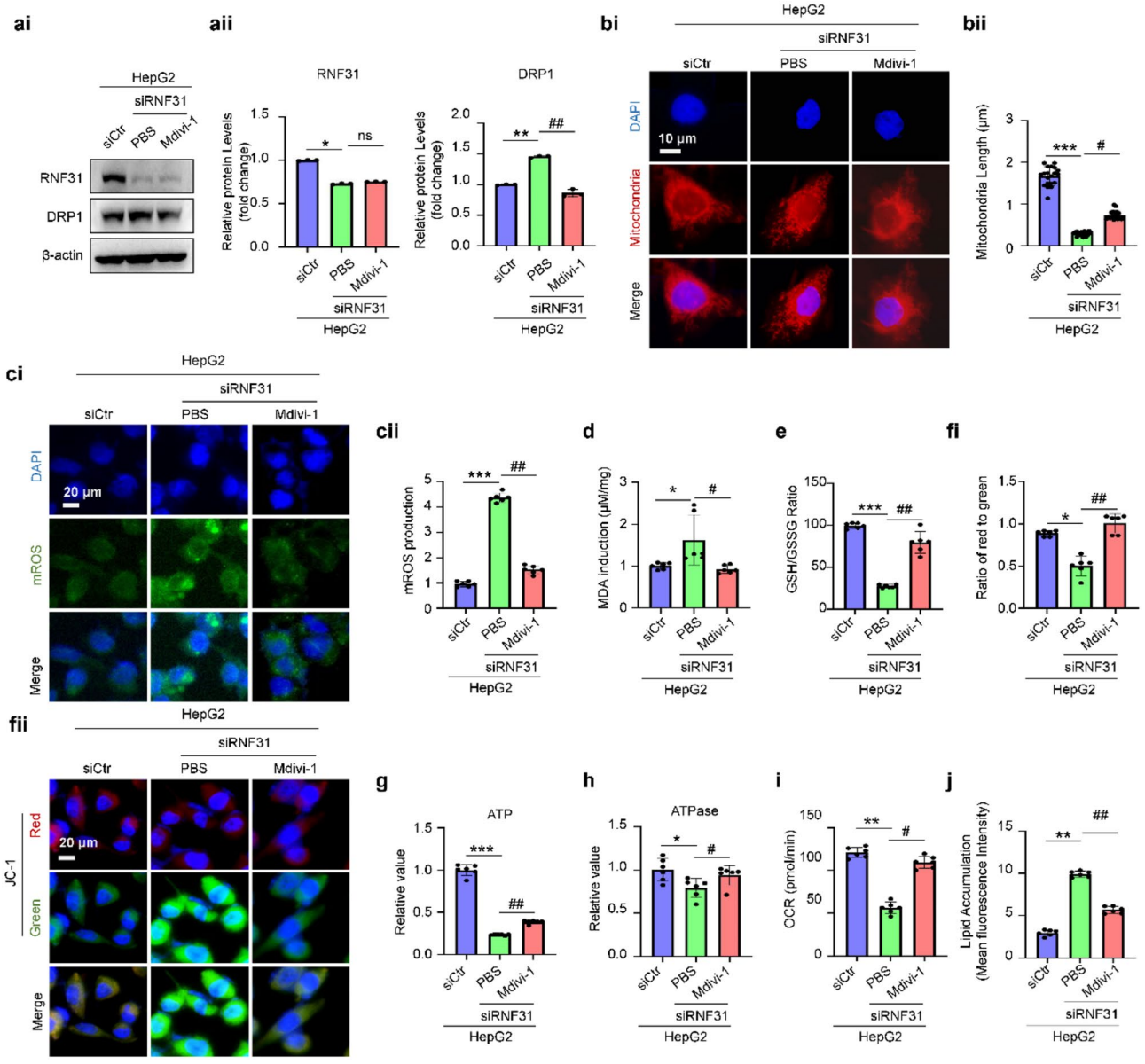

Fig. 5 DRP1 inhibition reverses the promotion effect of RNF31 knockdown on mitochondrial damage and lipid deposition in normal hepatocytes. **a** Western blot analysis of RNF31 and DRP1 protein expression in normal HepG2 cells transfected with siCtr, RNF31 siRNA with or without Mdivi-1 treatment for 24 h. ($n=3$; * $P<0.05$, ** $P<0.01$; ## $P<0.01$; ns, not significant). (Full-length blots are presented in Additional file 1, Fig. S11). **b** MitoTracker Deep Red staining and mitochondria length statistics in normal HepG2 cells transfected with siCtr, RNF31 siRNA with or without Mdivi-1 treatment for 24 h. Scale bar, 10 μm. ($n=6$; *** $P<0.001$; # $P<0.05$). **c** mROS staining in normal HepG2 cells transfected with siCtr, RNF31 siRNA with or without Mdivi-1 treatment for 24 h. Scale bar, 20 μm. ($n=6$; *** $P<0.001$; ## $P<0.01$). **d**, **e** MDA induction and GSH/GSSG ratio in normal HepG2 cells transfected with siCtr, RNF31 siRNA with or without Mdivi-1 treatment for 24 h. ($n=6$; * $P<0.05$, *** $P<0.001$; # $P<0.05$, ## $P<0.01$). **f** JC-1 staining of mitochondria membrane potential in normal HepG2 cells transfected with siCtr, RNF31 siRNA with or without Mdivi-1 treatment for 24 h. Scale bar, 20 μm. ($n=6$; * $P<0.05$; ## $P<0.01$). **g-i** The ATP content, ATPase activity, and OCR were measured in normal HepG2 cells transfected with siCtr, RNF31 siRNA with or without Mdivi-1 treatment for 24 h. ($n=6$; * $P<0.05$, ** $P<0.01$, *** $P<0.001$; # $P<0.05$, ## $P<0.01$). **j** Nile red staining of intracellular lipid droplets in normal HepG2 cells transfected with siCtr, RNF31 siRNA with or without Mdivi-1 treatment for 24 h. Scale bars, 50 μm. ($n=6$; ** $P<0.01$; ## $P<0.01$)

DRP1 and its regulated mitochondrial fission in lipotoxic hepatocytes in both in vivo and in vitro models, reducing mitochondrial dysfunction and lipid deposition. Additionally, the research findings indicate that RNF31 is a critical molecule in inhibiting hepatocyte lipid deposition by MSC-sEV and repairing HFD-induced liver tissue damage. RNF31 binds to and negatively regulates DRP1 gene expression, inhibiting mitochondrial fission and dysfunction.

Several studies have demonstrated that MSC-sEV can alleviate liver disease through its effects on lipid metabolism, inflammation, oxidative stress, and apoptosis at

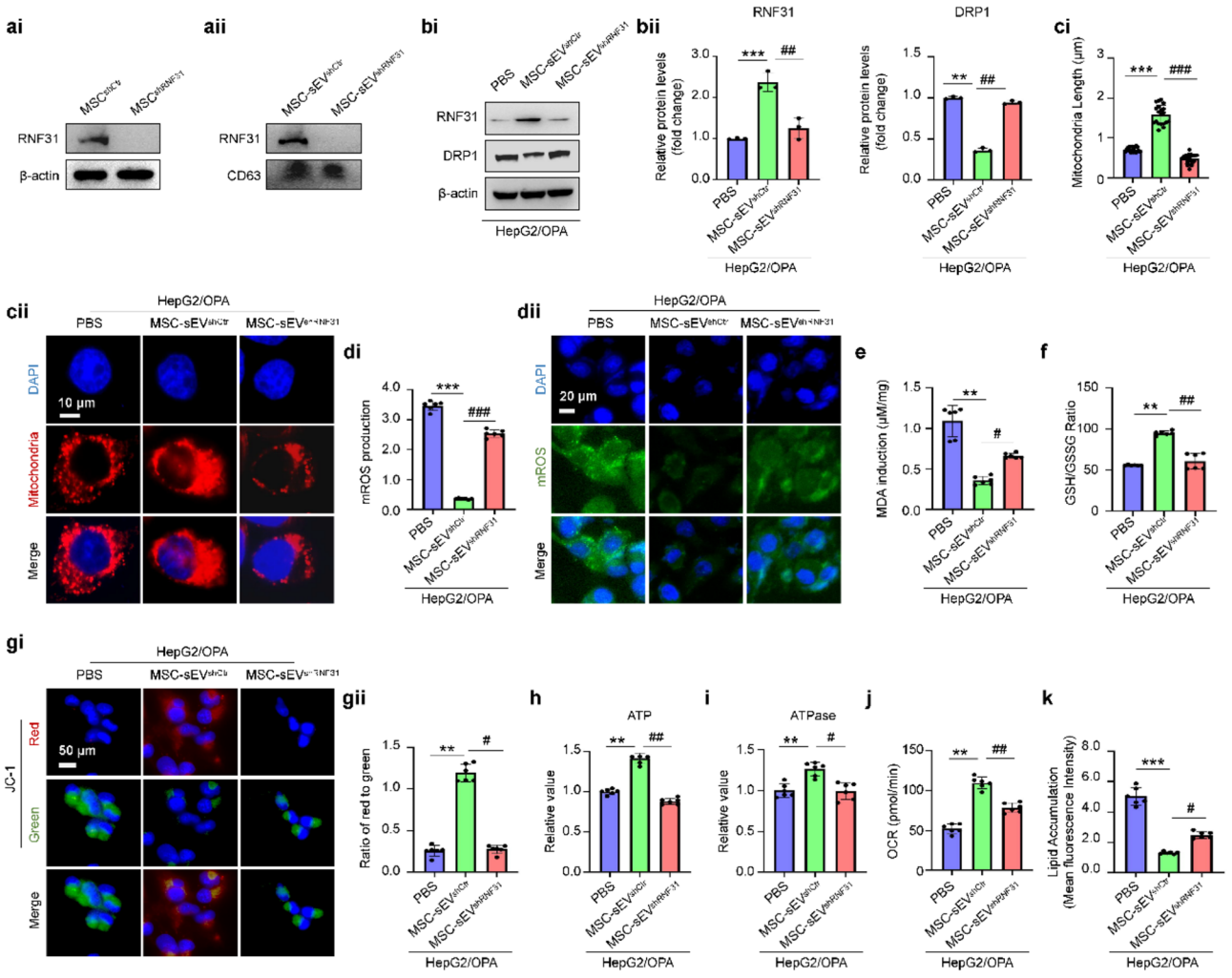

Fig. 6 Knockdown of RNF31 reduces the inhibitory effects of MSC-sEV on mitochondrial fission and lipid deposition in lipotoxic hepatocytes. **a** Western blot analysis of RNF31 protein expression in MSC^{shCtr}, MSC^{shRNF31}, MSC-sEV^{shCtr}, and MSC-sEV^{shRNF31}. (Full-length blots are presented in Additional file 1, Fig. S12). **b** Western blot analysis of RNF31 and DRP1 protein expression in OPA injured HepG2 cells treated with PBS, MSC-sEV^{shCtr} (800 μg/mL), and MSC-sEV^{shRNF31} (800 μg/mL) for 24 h ($n=3$; ** $P<0.01$; *** $P<0.001$; ## $P<0.01$). (Full-length blots are presented in Additional file 1, Fig. S13). **c** MitoTracker Deep Red staining and mitochondria length statistics in OPA-injured HepG2 cells treated with PBS, MSC-sEV^{shCtr} (800 μg/mL), and MSC-sEV^{shRNF31} (800 μg/mL) for 24 h. Scale bar, 10 μm. ($n=6$; *** $P<0.001$; ### $P<0.001$). **d** mROS staining in OPA-injured HepG2 cells treated with PBS, MSC-sEV^{shCtr} (800 μg/mL), and MSC-sEV^{shRNF31} (800 μg/mL) for 24 h. Scale bar, 20 μm. ($n=6$; *** $P<0.001$; ### $P<0.001$). **e**, **f** MDA induction and GSH/GSSG ratio in OPA-injured HepG2 cells treated with PBS, MSC-sEV^{shCtr} (800 μg/mL), and MSC-sEV^{shRNF31} (800 μg/mL). ($n=6$; ** $P<0.01$; # $P<0.05$, ## $P<0.01$). **g** JC-1 staining of mitochondria membrane potential in OPA-injured HepG2 cells treated with PBS, MSC-sEV^{shCtr} (800 μg/mL), and MSC-sEV^{shRNF31} (800 μg/mL). Scale bar, 50 μm. ($n=6$; ** $P<0.01$; # $P<0.05$). **h-j** The ATP content, ATPase activity, and OCR were measured in OPA-injured HepG2 cells treated with PBS, MSC-sEV^{shCtr} (800 μg/mL), and MSC-sEV^{shRNF31} (800 μg/mL). ($n=6$; ** $P<0.01$; # $P<0.05$, ## $P<0.01$). **k** Nile red staining of intracellular lipid droplets in OPA-injured HepG2 cells treated with PBS, MSC-sEV^{shCtr} (800 μg/mL), and MSC-sEV^{shRNF31} (800 μg/mL). Scale bar, 50 μm. ($n=6$; ***$P<0.001$; # $P<0.05$)

different stages of disease progression [21, 22, 40]. MSC-sEV has improved lipid accumulation in MASLD by activating AMPK, inhibiting SREBP-1 C-mediated fatty acid synthesis, and enhancing the PPARα-mediated fatty acid oxidation process [22]. Additionally, our previous study revealed that MSC-sEV can promote lipid peroxidation and mROS generation, thereby increasing LX-2 ferroptosis and alleviating liver fibrosis progression [21]. Building on these findings, this study also demonstrated that MSC-sEV can inhibit hepatocyte oxidative stress and lipid deposition. Excessive mitochondrial fission is crucial in mitochondrial dysfunction, abnormal lipid metabolism, and hepatocyte lipid deposition. However, the potential of MSC-sEV to inhibit lipid deposition by modulating mitochondrial fission requires further investigation. Our research results uncover a novel role of MSC-sEV in regulating mitochondrial fission for the repair of MASLD.

Targeting mitochondrial fission inhibition may hold promise as a therapeutic approach for various chronic liver diseases, including MASLD. Mdivi-1 is a potential inhibitor of DRP1 and mitochondrial fission. Mdivi-1

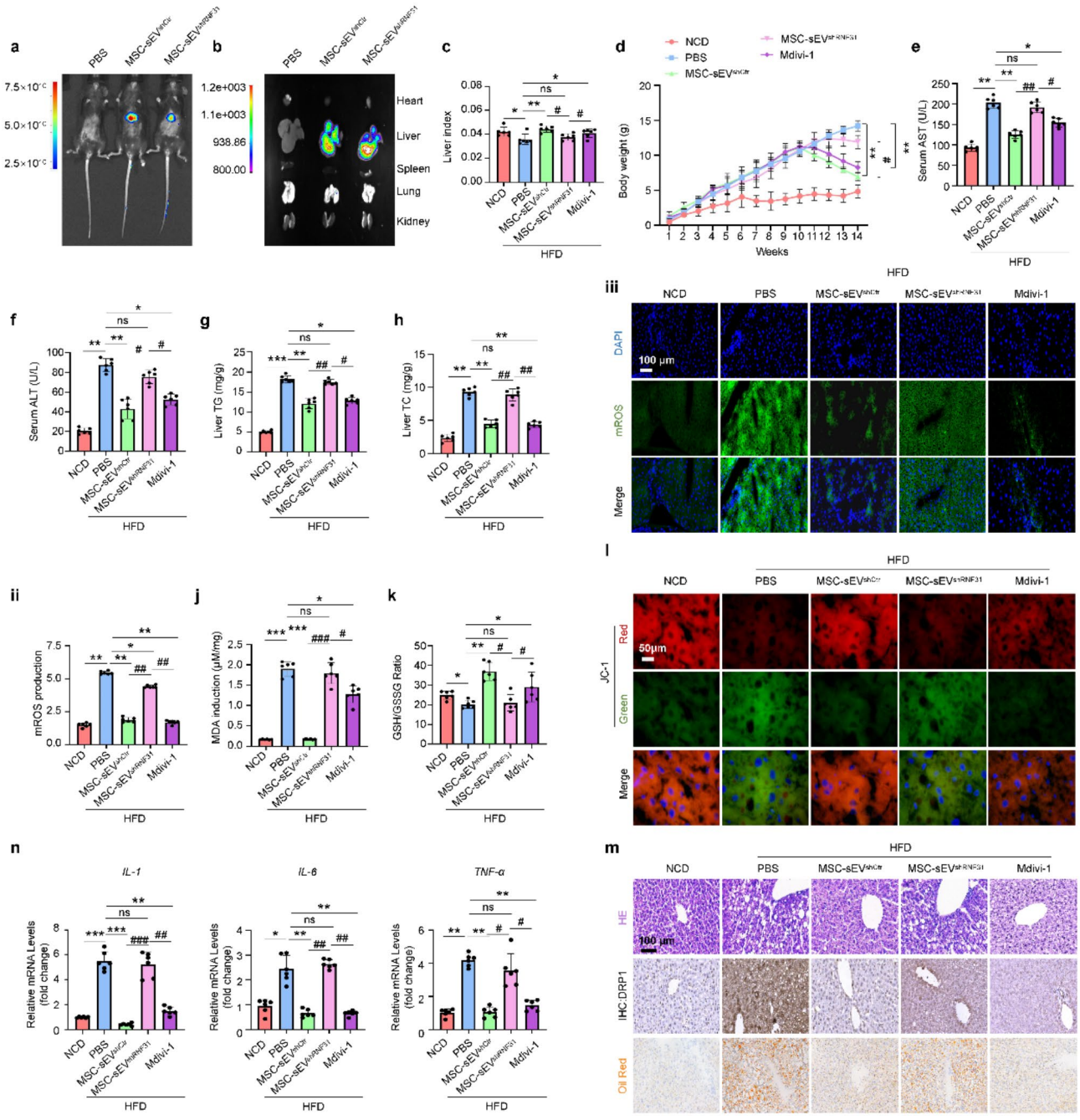

Fig. 7 Knockdown of RNF31 reduces the inhibitory effects of MSC-sEV on mitochondrial fission and lipid deposition in livers of HFD-fed mice. **a**, **b** Biodistribution of MSC-sEV in HFD-fed mice injected with PBS, MSC-sEV^{shCtr}, and MSC-sEV^{shRNF31} for 24 h. **c**, **d** Liver indexes (liver index = liver wet weight/body weight) and body weight changes from normal chow diet (NCD) fed mice, HFD-fed mice treated with PBS, MSC-sEV^{shCtr} (10 mg/kg), MSC-sEV^{shRNF31} (10 mg/kg), and Mdivi-1 (10 mg/kg). ($n = 6$; * $P < 0.05$; ** $P < 0.01$; # $P < 0.05$; ns, not significant). **e**, **f** Serum AST and ALT levels from mice in normal chow diet (NCD) fed mice, HFD-fed mice treated with PBS, MSC-sEV^{shCtr} (10 mg/kg), MSC-sEV^{shRNF31} (10 mg/kg), and Mdivi-1 (10 mg/kg) group. ($n = 6$; * $P < 0.05$; ** $P < 0.01$; # $P < 0.05$; ## $P < 0.01$; ns, not significant). **g**, **h** Liver TG (mg/g) and TC (mg/g) levels from mice in normal chow diet (NCD) fed mice, HFD-fed mice treated with PBS, MSC-sEV^{shCtr} (10 mg/kg), MSC-sEV^{shRNF31} (10 mg/kg), and Mdivi-1 (10 mg/kg) group. ($n = 6$; * $P < 0.05$; ** $P < 0.01$, *** $P < 0.001$; # $P < 0.05$; ## $P < 0.01$; ns, not significant). **i-k** mROS production, MDA induction, and GSH/GSSG ratio in livers from normal chow diet (NCD) fed mice, HFD-fed mice treated with PBS, MSC-sEV^{shCtr} (10 mg/kg), MSC-sEV^{shRNF31} (10 mg/kg), and Mdivi-1 (10 mg/kg). ($n = 6$; * $P < 0.05$, ** $P < 0.01$, *** $P < 0.001$; # $P < 0.05$, ## $P < 0.01$, ### $P < 0.001$; ns, not significant). **l** JC-1 staining of mitochondrial membrane potential in livers from normal chow diet (NCD) fed mice, HFD-fed mice treated with PBS, MSC-sEV^{shCtr} (10 mg/kg), MSC-sEV^{shRNF31} (10 mg/kg), and Mdivi-1 (10 mg/kg). Scale bar, 50 μm. **m** H&E staining, immunohistochemistry analysis of DRP1 protein, and Oil red O staining in livers from normal chow diet (NCD) fed mice, HFD-fed mice treated with PBS, MSC-sEV^{shCtr} (10 mg/kg), MSC-sEV^{shRNF31} (10 mg/kg), and Mdivi-1 (10 mg/kg). Scale bar, 100 μm. **n** Relative mRNA expression of IL-1, IL-6 and TNF-α in livers from normal chow diet (NCD) fed mice, HFD-fed mice treated with PBS, MSC-sEVshCtr (10 mg/kg), MSC-sEVshRNF31 (10 mg/kg), and Mdivi-1 (10 mg/kg) ($n = 6$; * $P < 0.05$, ** $P < 0.01$, *** $P < 0.001$; # $P < 0.05$, ## $P < 0.01$, ### $P < 0.001$; ns, not significant)

works by reducing the activation of DRP1, thereby decreasing the accumulation of mROS and mitochondrial DNA damage, ultimately preventing MASH [41]. Mdivi-1 treatment has been shown to inhibit lipid metabolism induced by high-fat, high-cholesterol, or methionine-choline-deficient diets, decrease macrophage infiltration in the injured liver, and promote macrophage polarization towards the M1 phenotype [42]. Moreover, Mdivi-1 can reduce the expression of fibrosis-related markers, such as Col1a1 and Acta2, and prevent liver fibrosis [38]. These studies highlight Mdivi-1 as a promising drug for the treatment of MASLD. In this study, we compared the inhibitory effects of MSC-sEV and Mdivi-1 on DRP1 and the repair of MASLD. The results indicated that MSC-sEV exhibited similar inhibitory effects on DRP1 expression, oxidative stress, and lipid deposition compared to Mdivi-1. These findings provide novel evidence and alternative options for targeting DRP1 in the repair of MASLD.

Research indicates that MSC-sEV plays a crucial role in tissue damage repair by transferring various active factors [43]. Previous studies also have demonstrated that MSC-sEV specifically targets liver tissue, primarily localizing within liver cells following injection [44, 45]. MSCs possess the capability to target damaged areas for repair [46]. MSC-sEV, produced paracrinely by MSCs and sharing similar properties, represent the primary mechanism through which MSCs exert their effects [20, 47]. This study demonstrates the enrichment of RNF31 in MSC-sEV and its delivery to lipotoxic hepatocytes in both in vivo and in vitro models. RNF31 was initially discovered in breast cancer cells and has since been associated with the progression of several human malignancies [48, 49]. However, the specific role of RNF31 in MASLD progression remains unclear. This study discovered that RNF31 interacted with DRP1 but not with FIS1 (another mitochondrial fission protein), and its overexpression or knockdown can regulate DRP1-mediated mitochondrial fission. This regulation reduces mitochondrial dysfunction, oxidative stress, and lipid deposition in lipotoxic-damaged hepatocytes. Additionally, we observed that RNF31 knockdown in MSC-sEV significantly impairs their ability to improve liver mitochondrial homeostasis and reduce lipid deposition. These findings uncover a novel role of RNF31 in regulating DRP1-mediated mitochondrial fission, highlighting RNF31 as a key active molecule in MSC-sEV repair of MASLD.

Our study has several limitations that need to be addressed. Firstly, further research is required to understand how RNF31 regulates the expression of DRP1 protein to decrease lipid deposition in hepatocytes. Recent investigations have shown that the ring finger domain of RNF31 has E3 ubiquitin ligase activity, which facilitates the ubiquitination of associated proteins and controls subsequent signal transduction [50]. Secondly, mitochondrial homeostasis is influenced by multiple proteins such as fusion proteins Mfn1 and Mfn2. Hence, it is essential to investigate the role of MSC-sEV and its impact on other mitochondrial biological processes associated with MASLD. Additionally, other regulatory factors might be present in MSC-sEV, which can be explored using protein chips and LncRNA-mRNA chips to uncover additional mechanisms through which MSC-sEV regulates and repair MASLD.

Conclusions

This study discovered that MSC-sEV can effectively suppress the expression of DRP1 and its regulated mitochondrial fission in lipotoxic hepatocytes. Additionally, RNF31 plays a crucial role in MSC-sEV's ability to reduce mitochondrial fission, mitigate hepatocyte lipid deposition, and repair liver tissue damage caused by a high-fat diet. These findings not only shed light on the novel role of RNF31 in regulating mitochondrial fission in lipotoxic hepatocytes but also provide a new perspective on the potential of MSC-sEV in targeting mitochondrial fission for the treatment of MASLD.

Abbreviations

Co-IP	Co-immunoprecipitation
de-MSC-sEV	sEVdepleted MSC culture medium
DRP1	Dynamin-related protein 1
GSH	Glutathione
H&E	Hematoxylin and Eosin
HFD	High-fat diet
MDA	Malondialdehyde
MSCs	Mesenchymal stem cells
MSC-sEV	MSC-derived small extracellular vesicles
MSC-sEV^{shRNF31}	RNF31 knockdown MSC-sEV
MASLD	Metabolic dysfunction-associated steatotic liver disease
OPA	Oleic acid and Palmitic acid
RNF31	RING finger protein 31
mROS	Mitochondrial reactive oxygen species
sEV	Small extracellular vesicles

Supplementary Information

The online version contains supplementary material available at https://doi.org/10.1186/s13287-025-04228-2.

Supplementary Material 1

Supplementary Material 2

Supplementary Material 3

Acknowledgements

The authors declare that they have not use AI-generated work in this manuscript.

Author contributions

Yifei Chen and Fuji Yang for the original draft's investigation, methodology, and writing. Yanjin Wang, Yujie Shi, Likang Liu, Wei Luo, and Jing Zhou for the Investigation, Methodology, and Data curation. Yongmin Yan is responsible for conceptualization, funding acquisition, project administration, and supervision.

Funding
This work was supported by the National Natural Science Foundation of China (Grant number 82272421), Changzhou's 14th five-year plan project to train high-level health professionals (Grant number 2022CZLJ027), Changzhou Special Program for the Introduction of Foreign Talents (Grant number CQ20240052). Open project of Jiangsu Provincial Key Laboratory of Key Laboratory of Laboratory Medicine (Grant number JSKLM-Z-2024-001), Key Project of Jiangsu Provincial Health Commission (Grant number K2024037).

Data availability
All data generated or used during the study appear in the submitted article.

Declarations

Consent for publication
Not applicable.

Competing interests
The authors declared no competing financial interest.

Ethics approval and consent to participate
All experiments involving animals were conducted according to the ethical policies and procedures approved by the Jiangsu University ethics committee (Approval no. UJS-IACUC-AP-2020033127). This study is reported in accordance with ARRIVE guidelines for animal experiments. The commercial HepG2 cells and LO2 cells used in this study were purchased from Fenghui Biology Co., Ltd. and identified using genotyping of STR loc by Shanghai Yihe Biotechnology Co., Ltd. (https://www.fenghbio.cn/goods.php?id=86043, https://www.fenghbio.cn/goods.php?id=85691). Fenghui Biology Co., Ltd has confirmed that ethical approval has been obtained for the collection of HepG2 and LO2 cells and that the donor has signed an informed consent form. The use of human umbilical cord tissues was approved by the Jiangsu University ethics committee (2012258). This project entitled "The effect and mechanism of engineered MSC exosomes targeting LSEC autophagy to inhibit hepatic sinusoidal capillarization" was approved on March 8, 2019. Furthermore, all patients signed the approved informed consent form, and all the procedures were performed in accordance with the principles of the Declaration of Helsinki.

Author details
[1]Department of Laboratory Medicine, Wujin Hospital Affiliated with Jiangsu University, Changzhou 213017, China
[2]Department of Laboratory Medicine, School of Medicine, Jiangsu University, Zhenjiang 212013, China
[3]Wujin Institute of Molecular Diagnostics and Precision Cancer Medicine of Jiangsu University, Changzhou 213017, China
[4]Changzhou Key Laboratory of Exosome Foundation and Transformation Application, Wujin Hospital Affiliated with Jiangsu University (Wujin Clinical College of Xuzhou Medical University, Changzhou 213017, China

Received: 22 November 2024 / Accepted: 11 February 2025
Published online: 05 March 2025

References

1. Spooner MH, Jump DB. Nonalcoholic fatty liver disease and Omega-3 fatty acids: mechanisms and clinical use. Annu Rev Nutr. 2023;43:199–223.
2. Younossi ZM. Non-alcoholic fatty liver disease - A global public health perspective. J Hepatol. 2019;70(3):531–44.
3. Brunt EM, Wong VW, Nobili V, Day CP, Sookoian S, Maher JJ, Bugianesi E, Sirlin CB, Neuschwander-Tetri BA, Rinella ME. Nonalcoholic fatty liver disease, Nature reviews. Disease Primers. 2015;1:15080.
4. Wester A, Hagström H. Risk of fractures and subsequent mortality in non-alcoholic fatty liver disease: a nationwide population-based cohort study. J Intern Med. 2022;292(3):492–500.
5. Cho Y, Chang Y, Ryu S, Wild SH, Byrne CD. Synergistic effect of non-alcoholic fatty liver disease and history of gestational diabetes to increase risk of type 2 diabetes. Eur J Epidemiol. 2023;38(8):901–11.
6. Zhang Y, Xia Z, Cai X, Su X, Jin A, Mei L, Jing J, Wang S, Meng X, Li S, Wang M, Wei T, Wang Y, He Y, Pan Y. Association of metabolic dysfunction-associated fatty liver disease with systemic atherosclerosis: a community-based cross-sectional study. Cardiovasc Diabetol. 2023;22(1):342.
7. Kokkorakis M, Muzurović E, Volčanšek Š, Chakhtoura M, Hill MA, Mikhailidis DP, Mantzoros CS. Steatotic liver disease: pathophysiology and emerging pharmacotherapies. Pharmacol Rev. 2024;76(3):454–99.
8. Yadav P, Singh SK, Rajput S, Allawadhi P, Khurana A, Weiskirchen R, Navik U. Therapeutic potential of stem cells in regeneration of liver in chronic liver diseases: current perspectives and future challenges. Pharmacol Ther. 2024;253:108563.
9. Liao N, Pan F, Wang Y, Zheng Y, Xu B, Chen W, Gao Y, Cai Z, Liu X, Liu J. Adipose tissue-derived stem cells promote the reversion of non-alcoholic fatty liver disease: an in vivo study. Int J Mol Med. 2016;37(5):1389–96.
10. Pan F, Liao N, Zheng Y, Wang Y, Gao Y, Wang S, Jiang Y, Liu X. Intrahepatic transplantation of adipose-derived stem cells attenuates the progression of non-alcoholic fatty liver disease in rats. Mol Med Rep. 2015;12(3):3725–33.
11. Seki A, Sakai Y, Komura T, Nasti A, Yoshida K, Higashimoto M, Honda M, Usui S, Takamura M, Takamura T, Ochiya T, Furuichi K, Wada T, Kaneko S. Adipose tissue-derived stem cells as a regenerative therapy for a mouse steatohepatitis-induced cirrhosis model. Hepatology. 2013;58(3):1133–42.
12. Qin L, Liu N, Bao CL, Yang DZ, Ma GX, Yi WH, Xiao GZ, Cao HL. Mesenchymal stem cells in fibrotic diseases-the two sides of the same coin. Acta Pharmacol Sin. 2023;44(2):268–87.
13. Qian H, Ding X, Zhang J, Mao F, Sun Z, Jia H, Yin L, Wang M, Zhang X, Zhang B, Yan Y, Zhu W, Xu W. Cancer stemness and metastatic potential of the novel tumor cell line K3: an inner mutated cell of bone marrow-derived mesenchymal stem cells. Oncotarget. 2017;8(24):39522–33.
14. Palamà MEF, Coco S, Shaw GM, Reverberi D, Ghelardoni M, Ostano P, Chiorino G, Sercia L, Persano L, Gagliani MC, Cortese K, Pisignano D, Murphy JM, Gentili C. Xeno-free cultured mesenchymal stromal cells release extracellular vesicles with a therapeutic miRNA cargo ameliorating cartilage inflammation in vitro. Theranostics. 2023;13(5):1470–89.
15. Yin K, Wang S, Zhao RC. Exosomes from mesenchymal stem/stromal cells: a new therapeutic paradigm. Biomark Res. 2019;7:8.
16. Lu X, Guo H, Wei X, Lu D, Shu W, Song Y, Qiu N, Xu X. Current Status and Prospect of Delivery Vehicle based on mesenchymal stem cell-derived exosomes in Liver diseases. Int J Nanomed. 2023;18:2873–90.
17. Hu C, Wu Z, Li L. Mesenchymal stromal cells promote liver regeneration through regulation of immune cells. Int J Biol Sci. 2020;16(5):893–903.
18. Huang W, Hong S, Zhu X, Alsaeedi MH, Tang H, Krier JD, Gandhi D, Jordan KL, Saadiq IM, Jiang Y, Eirin A, Lerman LO. Obesity blunts the effect of mesenchymal stem cell-derived extracellular vesicles. Kidney Int Rep. 2023;8(9):1841–51.
19. Sun Y, Shi H, Yin S, Ji C, Zhang X, Zhang B, Wu P, Shi Y, Mao F, Yan Y, Xu W, Qian H. Human mesenchymal stem cell derived exosomes alleviate type 2 diabetes Mellitus by reversing Peripheral insulin resistance and relieving β-Cell Destruction. ACS Nano. 2018;12(8):7613–28.
20. Psaraki A, Ntari L, Karakostas C, Korrou-Karava D, Roubelakis MG. Extracellular vesicles derived from mesenchymal stem/stromal cells: the regenerative impact in liver diseases. Hepatology. 2022;75(6):1590–603.
21. Tan Y, Huang Y, Mei R, Mao F, Yang D, Liu J, Xu W, Qian H, Yan Y. HucMSC-derived exosomes delivered BECN1 induces ferroptosis of hepatic stellate cells via regulating the xCT/GPX4 axis. Cell Death Dis. 2022;13(4):319.
22. Yang F, Wu Y, Chen Y, Xi J, Chu Y, Jin J, Yan Y. Human umbilical cord mesenchymal stem cell-derived exosomes ameliorate liver steatosis by promoting fatty acid oxidation and reducing fatty acid synthesis. JHEP Rep. 2023;5(7):100746.
23. Shi Y, Yang X, Wang S, Wu Y, Zheng L, Tang Y, Gao Y, Niu J. Human umbilical cord mesenchymal stromal cell-derived exosomes protect against MCD-induced NASH in a mouse model. Stem Cell Res Ther. 2022;13(1):517.
24. Zhang S, Wu Z, Shi L, Yan S, Huang Z, Lu B, Wang Z, Ji L. 3,5,4'-tetrahydroxystilbene-2-O-β-D-glucoside ameliorates NAFLD via attenuating hepatic steatosis through inhibiting mitochondrial dysfunction dependent on SIRT5. Phytomedicine: Int J Phytotherapy Phytopharmacology. 2022;2:153994.
25. Lee J, Park JS, Roh YS. Molecular insights into the role of mitochondria in non-alcoholic fatty liver disease. Arch Pharm Res. 2019;42(11):935–46.
26. Yu W, Wang X, Zhao J, Liu R, Liu J, Wang Z, Peng J, Wu H, Zhang X, Long Z, Kong D, Li W, Hai C. Stat2-Drp1 mediated mitochondrial mass increase is necessary for pro-inflammatory differentiation of macrophages. Redox Biol. 2020;37:101761.
27. Das N, Mandala A, Naaz S, Giri S, Jain M, Bandyopadhyay D, Reiter RJ, Roy SS. Melatonin protects against lipid-induced mitochondrial dysfunction in hepatocytes and inhibits stellate cell activation during hepatic fibrosis in mice. J Pineal Res. 2017;62(4).

28. Chen Y, Yang F, Shi Y, Sheng J, Wang Y, Zhang L, Zhou J, Jin Y, Yan Y. RNF31 alleviates liver steatosis by promoting p53/BNIP3-related mitophagy in hepatocytes. Free Radic Biol Med. 2024;219:163–79.
29. Marada A, Walter C, Suhm T, Shankar S, Nandy A, Brummer T, Dhaouadi I, Vögtle FN, Meisinger C. DYRK1A signalling synchronizes the mitochondrial import pathways for metabolic rewiring. Nat Commun. 2024;15(1):5265.
30. Qiao C, Xu W, Zhu W, Hu J, Qian H, Yin Q, Jiang R, Yan Y, Mao F, Yang H, Wang X, Chen Y. Human mesenchymal stem cells isolated from the umbilical cord. Cell Biol Int. 2008;32(1):8–15.
31. Xu W, Cui C, Cui C, Chen Z, Zhang H, Cui Q, Xu G, Fan J, Han Y, Tang L, Targher G, Byrne CD, Zheng MH, Yang L, Cai J, Geng B. Hepatocellular cystathionine γ lyase/hydrogen sulfide attenuates nonalcoholic fatty liver disease by activating farnesoid X receptor. Hepatology. 2022;76(6):1794–810.
32. Longhitano L, Distefano A, Amorini AM, Orlando L, Giallongo S, Tibullo D, Lazzarino G, Nicolosi A, Alanazi AM, Saoca C, Macaione V, Aguennouz M, Salomone F, Tropea E, Barbagallo IA, Volti GL. G. Lazzarino, (+)-Lipoic acid reduces lipotoxicity and regulates mitochondrial homeostasis and energy balance in an in vitro model of liver steatosis. Int J Mol Sci. 2023;24(19).
33. Yu Z, Li Q, Wang Y, Li P. A potent protective effect of baicalein on liver injury by regulating mitochondria-related apoptosis. Apoptosis: Int J Program cell Death. 2020;25(5–6):412–25.
34. Rivkin E, Almeida SM, Ceccarelli DF, Juang YC, MacLean TA, Srikumar T, Huang H, Dunham WH, Fukumura R, Xie G, Gondo Y, Raught B, Gingras AC, Sicheri F, Cordes SP. The linear ubiquitin-specific deubiquitinase gumby regulates angiogenesis. Nature. 2013;498(7454):318–24.
35. Matsunaga Y, Nakatsu Y, Fukushima T, Okubo H, Iwashita M, Sakoda H, Fujishiro M, Yamamotoya T, Kushiyama A, Takahashi S, Tsuchiya Y, Kamata H, Tokunaga F, Iwai K, Asano T. LUBAC formation is impaired in the livers of mice with MCD-Dependent nonalcoholic steatohepatitis. Mediators Inflamm. 2015;2015:125380.
36. Yamamotoya T, Nakatsu Y, Matsunaga Y, Fukushima T, Yamazaki H, Kaneko S, Fujishiro M, Kikuchi T, Kushiyama A, Tokunaga F, Asano T, Sakoda H. Reduced SHARPIN and LUBAC formation may contribute to CCl_4- or Acetaminophen-Induced Liver cirrhosis in mice. Int J Mol Sci.2017;18(2).
37. Yang H, Sibilla C, Liu R, Yun J, Hay BA, Blackstone C, Chan DC, Harvey RJ, Guo M. Clueless/CLUH regulates mitochondrial fission by promoting recruitment of Drp1 to mitochondria. Nat Commun. 2022;13(1):1582.
38. Elbadawy M, Tanabe K, Yamamoto H, Ishihara Y, Mochizuki M, Abugomaa A, Yamawaki H, Kaneda M, Usui T, Sasaki K. Evaluation of the efficacy of mitochondrial fission inhibitor (Mdivi-1) using non-alcoholic steatohepatitis (NASH) liver organoids. Front Pharmacol. 2023;14:1243258.
39. Zhang L, Xie X, Tao J, Wang S, Hu M, Wang X, Yu Z, Xu L, Lin Y, Wu W, Cheng J, Wu L, Liu W, Gao R, Wang J. Mystery of bisphenol F-induced nonalcoholic fatty liver disease-like changes: roles of Drp1-mediated abnormal mitochondrial fission in lipid droplet deposition. Sci Total Environ. 2023;904:166831.
40. Liu Y, Lou G, Li A, Zhang T, Qi J, Ye D, Zheng M, Chen Z. AMSC-derived exosomes alleviate lipopolysaccharide/d-galactosamine-induced acute liver failure by mir-17-mediated reduction of TXNIP/NLRP3 inflammasome activation in macrophages. EBioMedicine. 2018;36:140–50.
41. Quan Y, Shou D, Yang S, Cheng J, Li Y, Huang C, Chen H, Zhou Y. Mdivi1 ameliorates mitochondrial dysfunction in non-alcoholic steatohepatitis by inhibiting JNK/MFF signaling. J Gastroenterol Hepatol. 2023;38(12),2215–2227.
42. Liu X, Zhang X, Niu X, Zhang P, Wang Q, Xue X, Song G, Yu J, Xi G, Song L, Li Y, Ma C. Mdivi-1 modulates Macrophage/Microglial polarization in mice with EAE via the inhibition of the TLR2/4-GSK3β-NF-κB Inflammatory Signaling Axis. Mol Neurobiol. 2022;59(1):1–16.
43. Sun F, Sun Y, Wu F, Xu W, Qian H. Mesenchymal stem cell-derived extracellular vesicles: a potential therapy for diabetes Mellitus and Diabetic complications. Pharmaceutics. 2022;14(10).
44. Abdrakhmanov A, Gogvadze V, Zhivotovsky B. To eat or to die: deciphering selective forms of Autophagy. Trends Biochem Sci. 2020;45(4):347–64.
45. Ma N, Liu Y, Chen D, Wu C, Meng Z. In Vivo Imaging of Exosomes Labeled with NIR-II polymer dots in liver-injured mice. Biomacromolecules. 2022;23(11):4825–33.
46. Zhang L, Ma XJ, Fei YY, Han HT, Xu J, Cheng L, Li X. Stem cell therapy in liver regeneration: focus on mesenchymal stem cells and induced pluripotent stem cells. Pharmacol Ther. 2022;232:108004.
47. Varderidou-Minasian S, Lorenowicz MJ. Mesenchymal stromal/stem cell-derived extracellular vesicles in tissue repair: challenges and opportunities. Theranostics. 2020;10(13):5979–97.
48. Zhu J, Zhao C, Kharman-Biz A, Zhuang T, Jonsson P, Liang N, Williams C, Lin CY, Qiao Y, Zendehdel K, Strömblad S, Treuter E. Dahlman-Wright, the atypical ubiquitin ligase RNF31 stabilizes estrogen receptor α and modulates estrogen-stimulated breast cancer cell proliferation. Oncogene. 2014;33(34):4340–51.
49. Thompson HG, Harris JW, Lin L, Brody JP. Identification of the protein Zibra, its genomic organization, regulation, and expression in breast cancer cells. Exp Cell Res. 2004;295(2):448–59.
50. Zhu F, Yi G, Liu X, Zhu F, Zhao A, Wang A, Zhu R, Chen Z, Zhao B, Fang S, Yu X, Lin R, Liang R, Li D, Zhao W, Zhang Z, Guo W, Zhang S, Ge S, Fan X, Zhao G, Li B. Ring finger protein 31-mediated atypical ubiquitination stabilizes forkhead box P3 and thereby stimulates regulatory T-cell function. J Biol Chem. 2018;293(52):20099–111.

Publisher's note